Improvement and Validation of a Surgical Navigation Device for Arthroscopic Cartilage Repair

Undergraduate Honors Thesis

Presented in Partial Fulfillment of the Requirements for Graduation with Honors Research Distinction in the Department of Mechanical Engineering at The Ohio State University

By
Michael Francis Vignos

March, 2013

Thesis Committee: Robert Siston, PhD, Advisor
Alan Litsky, MD, ScD

Abstract

Knee articular cartilage defects are very painful and are presumed to be a precursor for osteoarthritis. Due its avascular nature, this tissue is unable to repair itself causing surgery to be the main option for treatment. Current surgical algorithms use defect area as the primary attribute to determine which procedure to use for each patient. Unfortunately, current techniques of calculating defect area are very poor, with errors ranging from -78.81% to 236.61% for surgeon area estimation, the current gold standard. Previously a cartilage navigation system was developed in our lab to improve surgeon accuracy in calculating defect area. However, when this system was used in cadaver knees it failed due to slipping of the surgical probe leading to a larger area calculation and tracing of the defect multiple times leading to a cumulative area calculation. The objectives of this project were to update the MATLAB code of the previous device to overcome these tracing errors, to develop new functions to increase the usability of the device, and to compare the use of this system to current area approximation techniques using shapes cut into plastic and artificial defects of known area. It was shown that this system produced more accurate area approximations than other current area approximation techniques with a significant decrease in error below that of use of a 5mm arthroscopic probe and use of a retractable arthroscopic probe. However, it was unable to reach the goal of less than 5% error. Modifications of this system are possible to further increase the accuracy of these area calculations. After these modifications are made, this system can be used by surgeons to quickly and accurately calculate the area of a cartilage defect. The use of that modified system may help them choose the proper procedure for each defect leading to better surgical outcomes for patients.

Acknowledgements

I would first off like to start by thanking my advisor, Dr. Rob Siston, for all of his help and support in this project. He was always there to help me brainstorm different aspects of this project, issues that arose, and provide new ideas on how to expand the project. I have always greatly appreciated the vision he has with his projects and this is one skill he has helped me begin to develop. This past year has been one of the busiest of my life so it was great to have an advisor that I could discuss all sorts of topics ranging from post-graduation plans to fellowships to Ohio State football.

I want to thank all of my NMBL lab mates for all of your assistance, support, and willingness to help test my device. I greatly appreciated all of your feedback on my presentations and your willingness to edit and review all sorts of documents for me. I also want to thank everyone else that helped me out with testing of my device. It was greatly appreciated!

I also want to thank Pete Brockmeier for providing a solid foundation for me to build my project off. Although I have never met Pete his work during his Master's gave me a great foundation for my project and I'm so thankful he commented his code because without that it probably would have taken me much longer to finish everything.

Most importantly I want to thank my parents for everything they have done for me. Without their support I never would have had the success I've experienced thus far in my life and during my four years in college. They have provided countless amounts of sacrifice in their life to help me get to where I am today. Nothing makes me happier than knowing I have made them proud.

I also want to thank all of my friends, especially Matt D'errico, Ben Jelen, and Charlie King. Without Matt and Ben alongside me I would have never been able to put the countless hours into studying and homework that I have during the past four years and Charlie has always been there to help support a little stress relief in my life.

Finally, I want to thank my girlfriend, Erica Loughry, for all of the love and support she has provided me since we first met. Meeting her three years ago truly changed my life and without her I probably would have never had the courage to take on a project of this magnitude. She has been willing to listen to all my complaining the past couple of years and I'm glad she has been willing to stick around through all of it.

Table of Contents

List of Figures

List of Tables

Chapter 1 : Introduction

1.1 Articular Cartilage

Articular cartilage is naturally found within the most mobile joints of the body. It is the glossy, white tissue that covers the end of the bones in synovial joints. This tissue provides a load bearing surface, force distribution, and a lubricated surface for articulation while experiencing virtually no wear when healthy (Setton et al., 1999). By doing so, it allows us to use these joints with smooth, pain-free motion.

Articular cartilage is extremely important for the normal, pain-free functioning of the knee. Experimental and mathematical studies of in vivo knee mechanics during various activities have revealed that forces in the knee can regularly reach 2.5 times body weight, and during physical activity these forces can be upwards of 4 times body weight (Komistek et al., 2005). Based on this, without knee cartilage we would be unable to perform both low and high intensity tasks pain free, ranging from walking and riding a bike to running and squatting.

Articular cartilage, like any other biological tissue, is made up of extracellular matrix and cells. For this tissue, the extracellular matrix is highly organized with chondrocytes (cartilage cells) spread sparsely throughout (Buckwalter et al., 2002). The components of the extracellular matrix consist of water, proteoglycans, type II collagen, and very low amounts of other proteins and glycoproteins (Figure 1.1). Water is present in the highest proportion in the tissue with it making up about 80% of the wet weight. This is followed by chondrocytes making up about 10%, proteoglycans and collagen combining to make up 9%, and the other molecules making up about 1% (Buckwalter et al., 2002). Articular cartilage is a unique tissue in that it contains no blood vessels, lymphatic vessels, or nerves. It also has a very low oxygen content and a low level of metabolic activity (Buckwalter et al., 2002). This attribute of articular cartilage is especially important when discussing damage of this tissue.

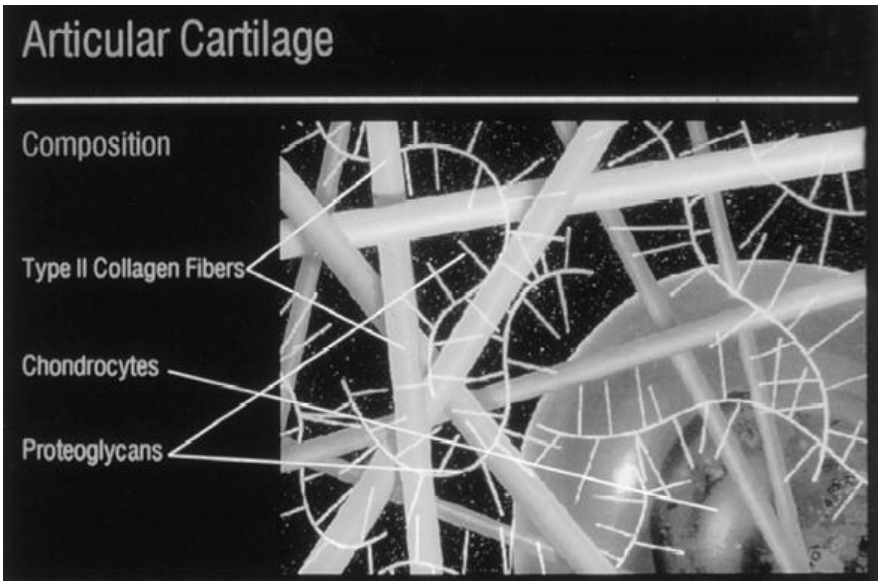

Figure 1.1: Composition of the articular cartilage matrix
As seen here, the articular cartilage matrix is comprised of Type II collagen fibers, chondrocytes, and proteoglycans. From Mandelbaum et al. 1998.

Each component of knee cartilage provides a different role that helps support the structure and function of the tissue. Chondrocytes initially form the components of the matrix and serve to repair and maintain it when small amounts of damage occur. The type II collagen serves as a shear-resisting structural support that opposes the tensile forces within the cartilage. The collagen meshwork also acts to hold the proteoglycans in place, which helps to maintain stability of the tissue. The proteoglycans in the matrix are negatively charged, which causes them to be hydrophobic (Figure 1.2). This hydrophobicity of the proteoglycans has two important consequences: the proteoglycans repel one another and attract water. These two consequences cause the tissue to expand and swell creating a hydrostatic pressure within the tissue. This hydrostatic pressure is essential for proper functioning of articular cartilage and allows the tissue to withstand the extremely large forces.

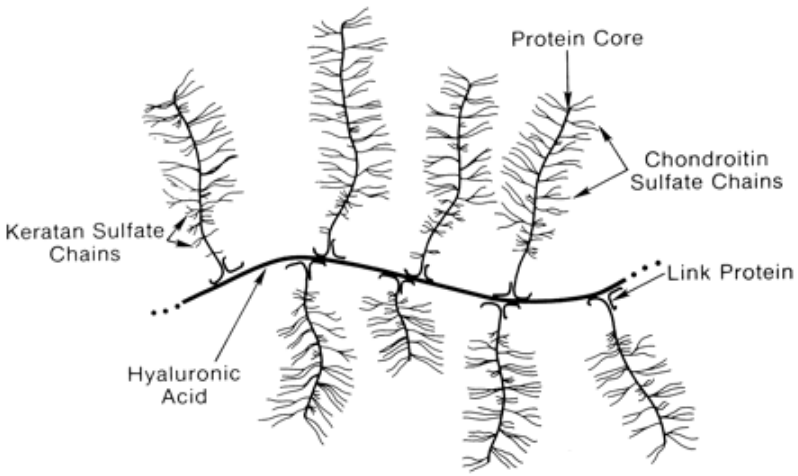

Figure 1.2: Proteoglycans composition within articular cartilage.
As seen in this image the proteoglycans repel each other causing them to be spread out. These proteoglycans also attract water causing the tissue to swell and create a hydrostatic pressure within the tissue. From Newman, 1998.

1.2 Articular Cartilage Defects

Since articular cartilage is so important to the proper function of the knee, damage to this tissue can be extremely problematic. Damage to cartilage within the knee is commonly seen as a cartilage defect. These defects are typically described as a "pothole" in the cartilage. Figure 1.3 shows that the defect disrupts the smooth surface of the cartilage and appears as if a piece of the cartilage has been removed. The missing section of cartilage modifies the structural integrity of the intact cartilage leading to stress concentrations around the defect rim and damage to the exposed subchondral bone. Both of these issues can lead to defect growth (Papaioannou et al., 2010; Pena et al. 2007; Dieppe, 1999)

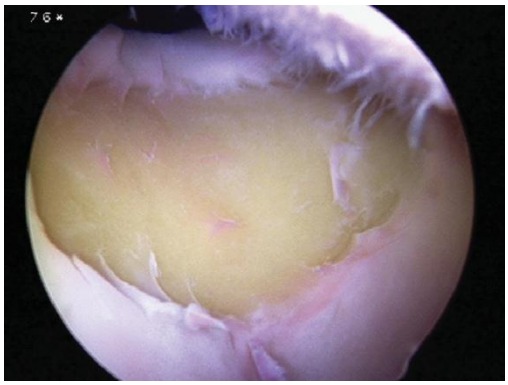

Figure 1.3: Arthroscopic image of an articular cartilage defect.
The defect is similar to a "pothole" in the cartilage and disrupts its functionality. Image courtesy of Dr. David Flanigan.

It is not completely understood how these defects occur, but it is believed that patients with minor knee trauma and repetitive joint loading are more susceptible (Flanigan et al., 2010). It is believed that they can result from high-loading and torsion impacts (Hinton et al., 2002) and often occur following injuries which shift loading patterns or cause misalignment of the tibiofemoral joint, such as ligament or meniscus tears (Hjelle et al., 2002; Mandelbaum et al., 1998). During knee arthroscopies of patients that have experienced knee injury, incidence of cartilage defects has been reported to be as high as 65% (Aroen et al., 2002; Hjelle et al., 2002; Shah et al., 2007; Curl et al., 1997). These defects are also very common in active populations, with an estimated 36% of all athletes between the ages of 27 to 47 years having at least one full thickness knee cartilage defect (Flanigan et al., 2010).

Articular cartilage defects are very problematic for patients. Patients with these defects have a wide-range of complications mainly associated with pain caused by the defect. These consist of pain during normal daily activities, such as walking, climbing stairs, or jogging, loss of range of motion, or joint locking or giving way (Aroen et al., 2002). Possibly the most problematic consequence of cartilage defects is that they are believed to be one of the major factors leading to knee osteoarthritis (Drawer et al., 2001; Cole et al., 2009). Osteoarthritis (OA) is a degenerative joint disease marked by knee pain and stiffness (Cain et al., 2001). Patients with OA experience a number of problems, including severe pain and disability, difficulty during activities of daily living, and quadriceps weakness (Jette et al., 1980; Fisher et al., 1991; Fisher and Pendergast, 1997). The complications associated with OA can be so severe that this disease typically results in a total knee replacement (Hinton et al., 2002).

1.3 Cartilage Repair Techniques

Since defects in mature cartilage do not heal, they require surgical repair, and a number of different procedures have developed to treat these defects. These consist of lavage and debridement, microfracture, osteochondral transplantation, and autologous chondrocyte implantation.

Lavage and debridement are the least technically demanding approaches and are typically used as the first step in a cartilage repair procedure. This procedure is performed arthroscopically and serves to remove the fragmented cartilage within the joint and clean up the fibrillated cartilage in order to create pain relief (Figure 1.4) (Gill et al., 2006; Lewis et al. 2006). This procedure is successful as an initial solution, but typically does not have successful results in the long term or for patients planning to live an active lifestyle following the surgery (Lewis et al. 2006).

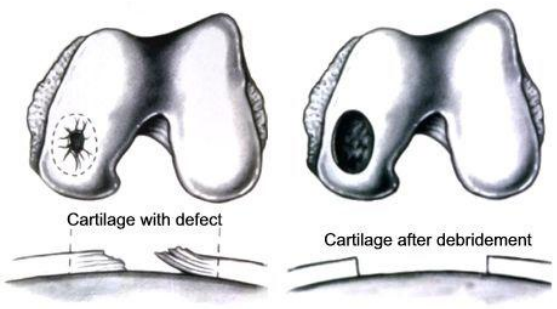

Figure 1.4: Cartilage defect before and after debridement.
During debridement the fibrillated cartilage is removed to smooth of the edges of the defect in an attempt to prevent expansion of the defect and to reduce patient pain. From Jordan 2001.

Microfracture is a marrow-stimulating technique that attempts to generate new cartilage to fill in the defect. This is an arthroscopic procedure in which surgeons use a special tool, called an awl, to create tiny, evenly spaced holes in the exposed subchondral bone. By creating these holes the surgeons induce bleeding within bone (Figure 1.5). This bleeding attempts to take advantage of the pluripotent mesenchymal stem cells that reside within the bone marrow (Steadman 2001). These stem cells fill in the defect and are intended to differentiate into chondrocytes to generate new cartilage. However, this approach is unable to produce hyaline (articular) cartilage and instead results in fibrocartilage (Steadman 2001).

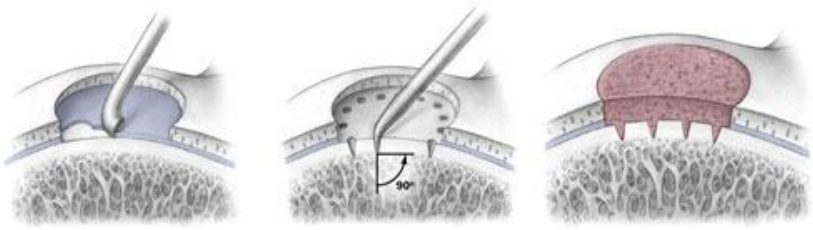

Figure 1.5: Steps of microfracture.
(A) Removing the calcified cartilage to expose the subchondral bone. (B) Using an awl to make 3-4 mm, evenly spaced holes in the subchondral bone. (C) Filling of the defect with marrow containing pluripotent mesenchymal stem cells. From Mithoefer et al., 2005.

Osteochondral transplantation is a form of cartilage replacement and consists of two sub-techniques: osteochondral autograft transplantation and osteochondral allograft transplantation (Memon et al., 2012). In autograft transplantation, a cylindrical plug of subchondral bone and cartilage is removed from a healthy, minimally weight-bearing region of the patient's knee (Figure 1.6). It is then placed in the defect region where a hole of a slightly smaller diameter has been created (Lewis et al., 2006). This technique can be expanded to fill a much larger defect area, in which it is then called mosaicplasty. In mosaicplasty the same general technique is used except multiple bone plugs are harvested and transplanted from the undamaged cartilage to the damaged cartilage. These multiple bone plugs are then used to fill in the larger defect area (Figure 1.7) (Lewis et al., 2006). In allograft transplantation the technique is exactly the same except the bone plugs are taken from a cadaver specimen, as opposed to from the patient. In a successful osteochondral transplantation procedure, the graft becomes completely integrated with the adjacent bone and cartilage (Lewis et al., 2006).

Figure 1.6: Osteochondral bone plug.
This plug contains a section of subchondral bone on the bottom and a section of healthy cartilage on the top. Bone plugs similar to this one are used in osteochondral transplantation. From Marcus, 2013.

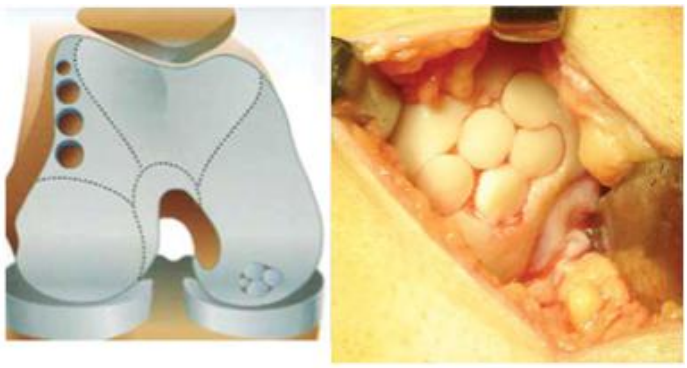

Figure 1.7: Mosaicplasty
Animated image of mosaicplasty of the left and actual image of mosaicplasty on the right. In both images it can be seen that multiple osteochondral plugs are used to fill the defect of a larger area. From Andrades, et al. 2011.

Autologous chondrocyte implantation (ACI) is currently a two-stage technique that attempts to regenerate completely new hyaline cartilage within the defect site. During the first stage a cartilage biopsy is performed, with a sample being taken from a non-weight bearing region of the knee. This biopsy is cultured and the chondrocytes are isolated (Riegger-Krugh et al., 2008). These cells are cultured for several weeks to generate enough chondrocytes to fill the defect area. Once enough chondrocytes are present the second stage occurs in which a periosteal flap or an artificial tissue membrane slightly larger than the size of the defect is sutured over the defect site (Riegger-Krugh et al., 2008). The cultured chondrocytes are then injected into the defect site and are intended to generate new hyaline cartilage (Figure 1.8).

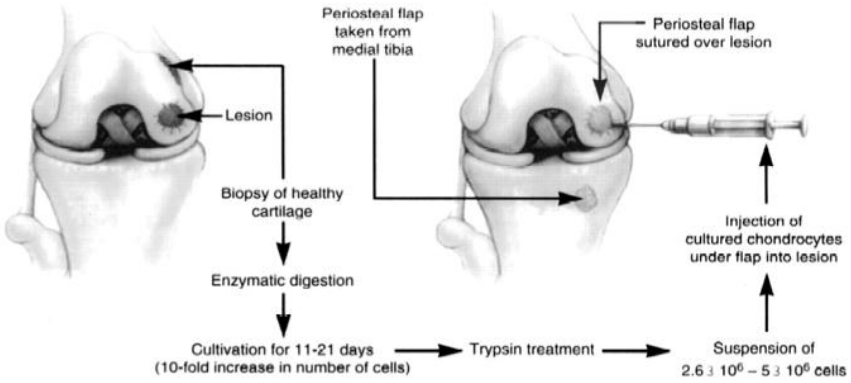

Figure 1.8: Steps involved in autologous chondrocyte implantation.
The main steps of this procedure include: a cartilage biopsy is extracted from the healthy cartilage, chondrocytes are extracted and cultured, a periosteal flap is sewn over the defect site, and the chondrocytes are injected into the defect. From Mandelbaum et al., 1998.

When determining which of the above procedures to use to repair a specific defect most current surgical algorithms use the cross-sectional area of the defect as the most critical factor. Most of these algorithms site 2 cm^2 as the threshold between simpler marrow-stimulation techniques and more complex cartilage restoration techniques (Cain et al., 2001; Scott, 2005; Alford and Cole, 2005; Clark et al. 2005; Farr et al. 2004; Scopp and Mandelbaum, 2004). Defects smaller than 2 cm^2 are generally treated with microfracture or osteochondral autografting, while larger defects are treated with ACI or osteochondral allografting (Figure 1.9). Although this critical defect size has become widely accepted clinically, there is little biomechanical evidence to support its use.

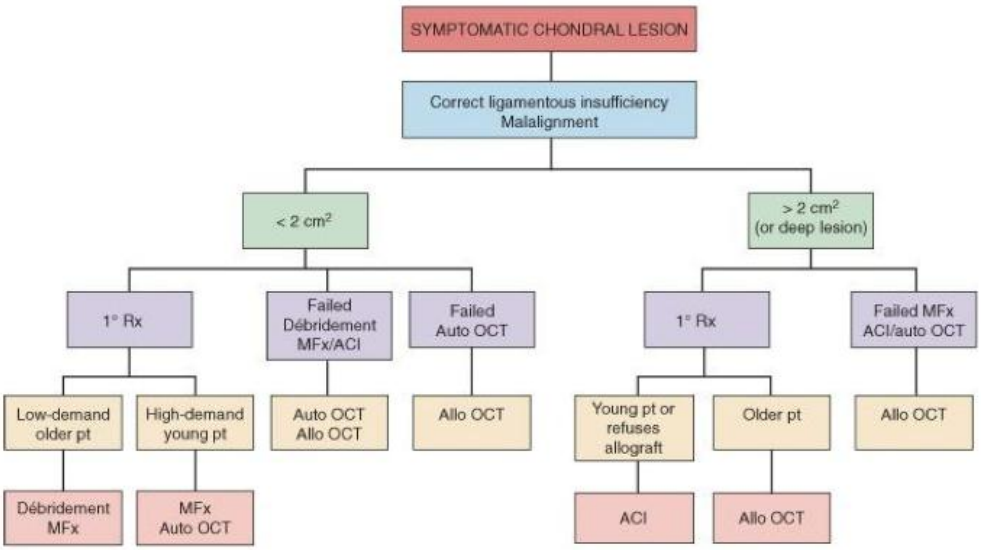

Figure 1.9: Surgical Algorithm Flow Chart.
Flow chart diagram showing the algorithm used by surgeons to choose the correct cartilage repair procedure for each patient. As seen in this diagram, the defect cross-sectional area is the determining factor between simpler marrow-stimulating techniques and more complex cartilage restoration techniques. Similar surgical algorithms are cited by many individuals (Cain et al., 2001; Scott, 2005; Alford and Cole, 2005; Clark et al. 2005; Farr et al. 2004; Scopp and Mandelbaum, 2004).

In order to perform this important defect area calculation there are two main techniques that are currently used. The current gold standard is to estimate the defect area during arthroscopic examination. In this approach surgeons use either surgical probes with tips of a known length or tools with markings of known length to measure various lengths on the defect (Figure 1.10). Once these lengths are known they estimate the defect area, typically by approximating it as a circle or an ellipse.

Figure 1.10: Area estimation during arthroscopic examination.
Examples of using arthroscopic tools to estimate the cross-sectional area of the defect. (A) A probe with evenly spaced markings used to measure the distance across the defect. (B) A probe with a tip of known length being used to measure lengths on the defect. Image courtesy of Dr. David Flanigan.

The other technique is to use pre-operative magnetic resonance imaging (MRI). In this technique MRI images are taken of the patient's knee prior to surgery and a three dimensional reconstruction of the patient's cartilage is generated using external software (Figure 1.11). The defect area is then estimated from this reconstruction.

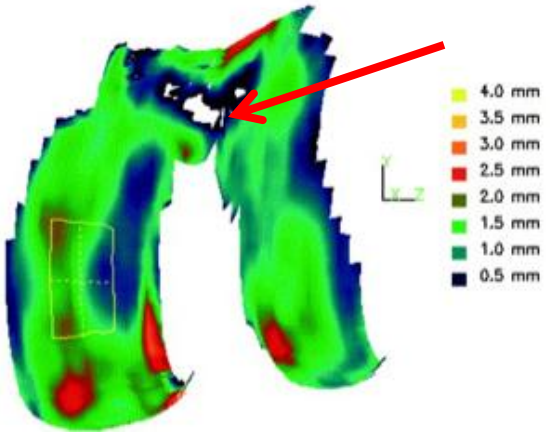

Figure 1.11: Three-dimensional cartilage defect reconstruction.
Three-dimensional reconstruction of the femoral cartilage of a cadaver specimen used to estimate the area of a cartilage defect. A defect created in the cartilage can be seen at the top of the reconstruction, denoted by the red arrow. The color on the reconstruction represents the thickness of the cartilage at that location. From McGibbon and Trahan, 2003.

Unfortunately both of these sizing techniques have been shown to be relatively inaccurate in estimating the actual size of the defect area. Siston et al. showed that estimation of defect size using arthroscopy produced errors ranging from an overestimation of 236.61% to an underestimation of -78.81% (Siston et al., 2013). This same study also showed that by using the arthroscopic examination technique only 57% of the defect size estimations would have led surgeons to choose the correct procedure, based

on current algorithms (Siston et al., 2013).

Current studies investigating the use of MRI to estimate defect area are limited in that the majority of them compare the measurements made by MRI to those made by arthroscopy, since arthroscopy is viewed as the gold standard. However, one study did compare the MRI estimations to the actual defect area and showed that defect size estimations from three-dimensional reconstructions can produce errors of up to 42% (Graichen et al., 2005). While these errors are smaller than that of arthroscopic examinations, this study was performed on defects created by punching circular holes in the cartilage. Cartilage defects are rarely perfect circles so using this technique may generate larger errors in a clinical setting. Also, as previously stated, defect lavage and debridement is typically the first step performed in a defect repair procedure. This increases the area of the defect, which means the estimations from pre-operative MRIs typically are an underestimation of the final area of the defect. This was shown in one study in which the final defect area was 65% larger than the pre-operative defect area predicted by MRI, causing this technique to be less effective in a clinical setting (Gomall et al., 2011). With these large errors in defect area estimation there presents a need for a new, more accurate, approach to determining this important defect attribute.

1.4 Surgical Navigation Systems

Currently there exists a class of tools that can help surgeons perform procedures in a more accurate and a more reproducible manner. Computer-assisted surgery (CAS) is defined as any computer-based procedure that uses technologies such as 3D imaging and real-time sensing in the planning, execution and follow-up of surgical procedures (Siston, 2005). CAS provides better visualization, improved targeting of sites, and improved diagnostic abilities for surgeons, which provides major advantages over conventional techniques.

One specific type of CAS is known as the surgical navigation system. These systems have been

developed to allow for spatial monitoring of important portions of the patient's body and of instrumented tools, so surgeons can track the movement of the surgical tools relative to the body parts of interest throughout the procedure (Siston et al., 2007; Diaz and Albright, 2008). Each surgical navigation system is made up of three general tools that allow the system to perform this tracking function (Figure 1.12). The first is the optical tracking camera. This is a camera that is able to track the position of small, metallic-colored optical tracking spheres (Figure 1.12) and relay the location of each of the spheres to the computer. The second tool is the optical tracker. Each optical tracker has a specific number of tracking spheres spaced in different orientations, which allows the camera to distinguish these tools from one another. These optical trackers allow the camera to monitor the spatial location of the body parts of interest and the spatial relationship of the body parts and the surgical tools. The third tool is the instrumented surgical device. By attaching tracking spheres to surgical devices, the camera is able to track the location of these tools as the procedure is performed.

Figure 1.12: Surgical navigation system tools.
(Top) Optical tracking camera used to track the three-dimensional position of optical tracking spheres. (Bottom Left) Instrumented surgical tool with optical tracking spheres attached. (Bottom Right) Optical trackers, which are attached to the patient's body to track specific body parts of interest. Images courtesy of Brockmeier, 2009.

Surgical navigation systems have been developed for use in many different procedures. These include applications in neurosurgery, oral and maxillofacial, ear, nose, and throat (ENT), orthopaedic, and visceral procedures (Medtronic, 2012). The major advantage of these systems is that they allow for accurate and complex measurements to be performed with only simple inputs into the software program.

For example, in navigation systems used for total joint replacements, software algorithms perform complex calculations real time that can be used to help guide surgical bone cuts. This can allow for a more accurate and a more repeatable surgical procedure to be performed (Siston et al., 2007).

The accuracy and repeatability created through the use of surgical navigation systems makes it a perfect choice for improving the current inability to properly size articular cartilage defects. As previously stated the current techniques to perform this size calculation are far too inaccurate, especially since defect size is considered the most important defect attribute. By creating a cartilage surgical navigation system we will be able to greatly improve the ability of surgeons to quickly and accurately calculate the area of a cartilage defect.

1.5 Previously Developed Surgical Navigation System

To take advantage of the capabilities surgical navigation systems present, a custom-built surgical navigation device was previously built in our research laboratory (Brockmeier, 2009). This system was designed to calculate the defect area, shape, orientation, and location of a femoral cartilage defect, as well as the curvature of the femoral condyle at the defect region (Brockmeier, 2009). Besides defect area, defect shape, orientation, location, and femoral condyle curvature were chosen to be calculated based on previous studies showing that these may also be important indicators of defect severity (Brockmeier et al. 2009; Flanigan et al. 2010). The technique to use this device involved using a surgical probe (Figure 1.13) to trace the border of the cartilage defect and from this tracing calculate the area of the defect. The system was validated on shapes of known area cut into a plastic sheet and artificial defects cut into Sawbones knees (Figure 1.14) and proved to be fairly accurate with an average error of only -0.36 ± 0.37 cm^2.

Figure 1.13: Probe used for previous surgical navigation system.
This probe was used to trace around the boundary of the defect to generate a two-dimensional polygon representative of the defect. Image courtesy of Brockmeier, 2009.

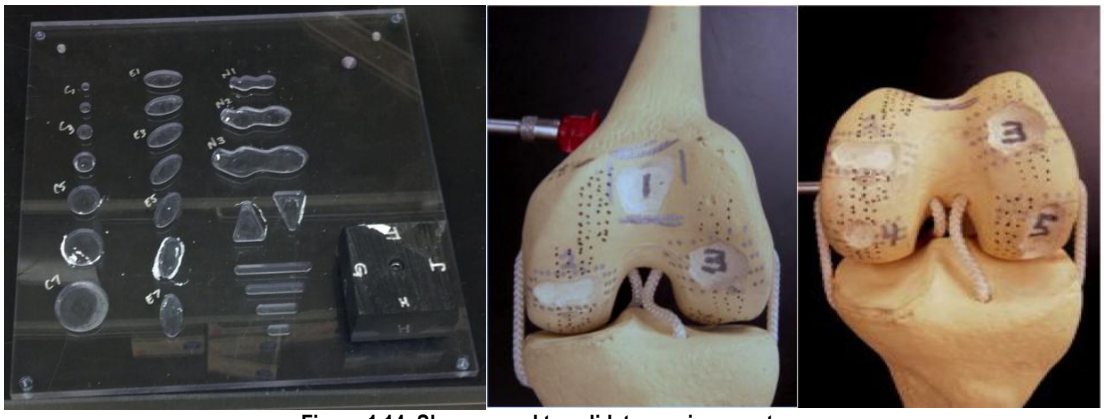

Figure 1.14: Shapes used to validate previous system.
(Left) Plastic sheet with shapes of known area etched in it. (Center and Right) Two views of a Sawbones knee with artificial defects etched into it. This plastic sheet and Sawbones knee were used to validate the previously developed surgical navigation system. Images courtesy of Brockmeier, 2009.

However, when this system was used by orthopaedic surgeons to determine the area of defects in the cartilage of cadaver knees two main issues arose (Figure 1.15). The first issue was since the subchondral bone was so rough from deterioration and since the knee is irrigated with water during arthroscopic examination it made it very difficult for surgeons to keep the probe tip directly on the defect edge during tracing. The probe tip would slip off the defect edge, causing the area generated by the tracing to be very different than the actual area of the defect. The second issue was that since surgeons were unable to accurately capture the geometry of the defect during tracing they wanted to trace the defect multiple times in an attempt to capture all the details. While capturing all the details of the defect is desirable, the approach that the navigation system was using to calculate the defect area caused the

cumulative area of each tracing to be calculated, rather than combining them into a single area.

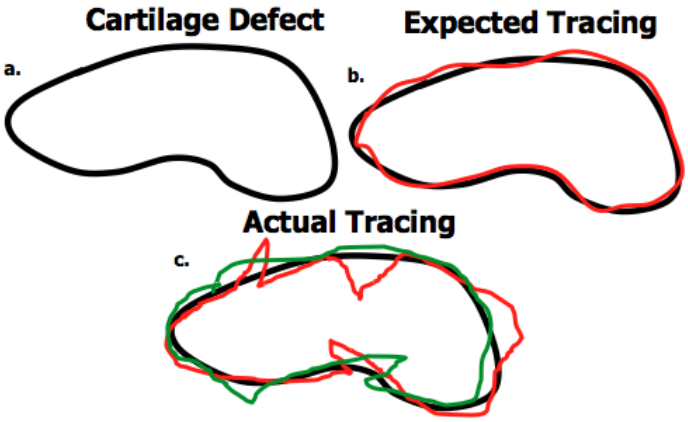

Figure 1.15: Images representing the possible cartilage tracing done by surgeons.
a. A general articular cartilage defect. **b.** An ideal tracing. This type of tracing was expected when the system was first developed. Note: This defect was only traced once. **c.** Example of an actual tracing encountered when device was tested in cadavers. This defect was traced around two times (red vs. green) and the tracing pattern contains many slips and diversions from the defect boundary. The goal of the system is to be able to calculate the size of the defect even when errors like this occur.

1.6 Focus of thesis

The focus of this thesis is on the improvement, testing, and validation of this previously developed surgical navigation device used to intra-operatively calculate multiple important attributes of articular cartilage defects. This project was motivated by the need for a new approach to calculating defect area, based on the inaccuracies of the current approaches. The main issues with this system were present in the custom-built MATLAB code. The objectives of this project were to first improve the MATLAB code to overcome the issues of the previous system and to create new functions to increase the ease-of-use of the system. After this was complete the system was validated on plastic shapes of known area and artificial defects cut into Sawbones knees. This project encompasses experimental biomechanics research, software and user interface design, and mechanical design.

1.7 Overview of Thesis

This thesis contains four chapters. Chapter 2 provides an overview of the cartilage navigation system, along with a description of the additions and improvements to the system. Chapter 3 discusses the

validation study performed to investigate the accuracy of this system at calculating the cross-sectional area of defects. Chapter 4 provides a summary of the project, along with future work and additional applications of this cartilage navigation system. References and an appendix are provided at the end.

Chapter 2 : Development of Cartilage Surgical Navigation System

2.1 Overview of Cartilage Surgical Navigation System

The cartilage surgical navigation system was designed using MATLAB R2012a (The Mathworks, Version 7.14, Natick, MA) with its graphical user interface development environment (GUIDE). GUIDE provides a set of tools for users to easily develop a visually appealing graphical user interface (GUI). This GUI is saved as a FIG-file and has an associated M-file, which contains the functions the GUI calls. The GUI provides the capability for surgeons to directly interact with the navigation system. On the GUI there are different buttons that the user must press in order to calibrate the system, to select and perform different data collection functions, and to export data from the system. When each of these buttons is pressed it calls the function associated with the button.

In order to begin using the cartilage surgical navigation system surgeons must perform 4 preliminary steps to prepare the system for data collection (Figure 2.1). The first step is to initialize the system. This initialization process simply requires surgeons to press a button (Figure 2.2). Once this button is pressed the computer begins data communication with the optical tracking camera, which is a Hybrid Polaris Spectra (NDI, Waterloo, Ontario, Canada). This optical tracking camera has a sampling rate of 60 Hz and is able to determine the three dimensional location of both passive and active markers with an accuracy of 0.25 mm RMS (Northern Digital, Inc., 2008).

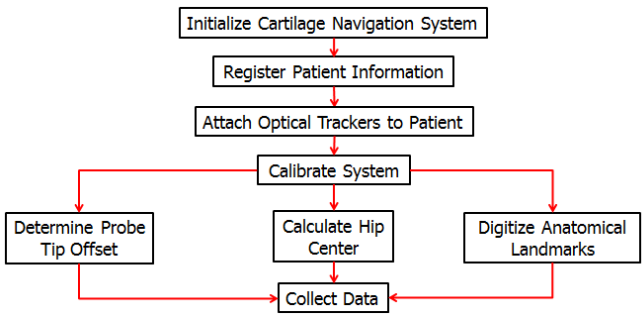

Figure 2.1: System set-up flow chart.
Flow chart representing steps that need to be taken before the system can be used to collect data.

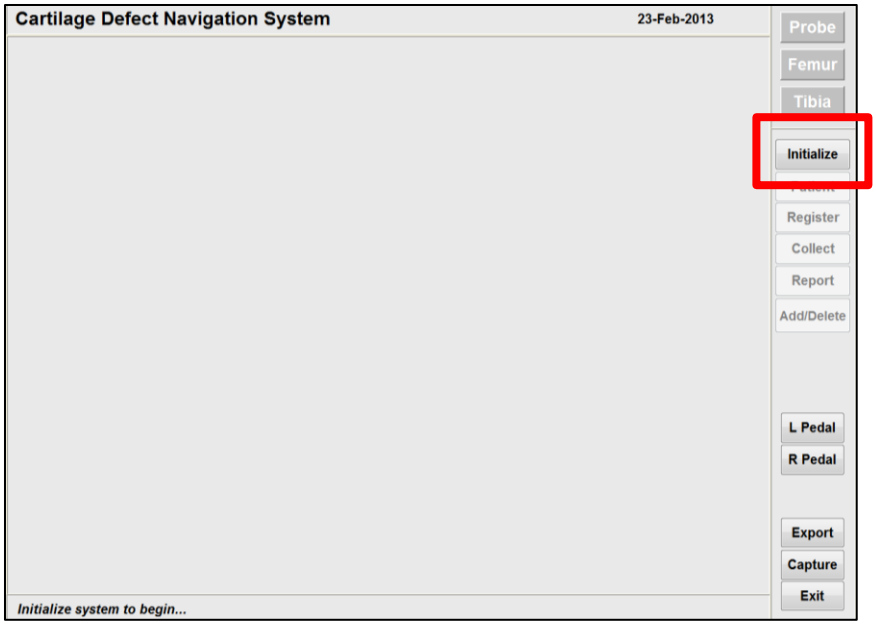

Figure 2.2: Initialization Panel

To initialize the system the user must press the initialize button to open communication between the computer and the optical tracking camera.

The second step is to register patient specific information, both about the patient and the defect (Figure 2.3 and Figure 2.4). These include patient demographics, the location of the defect on the femur, and a brief description of the defect. This step also gives surgeons the option to select a file location to save the data from the procedure.

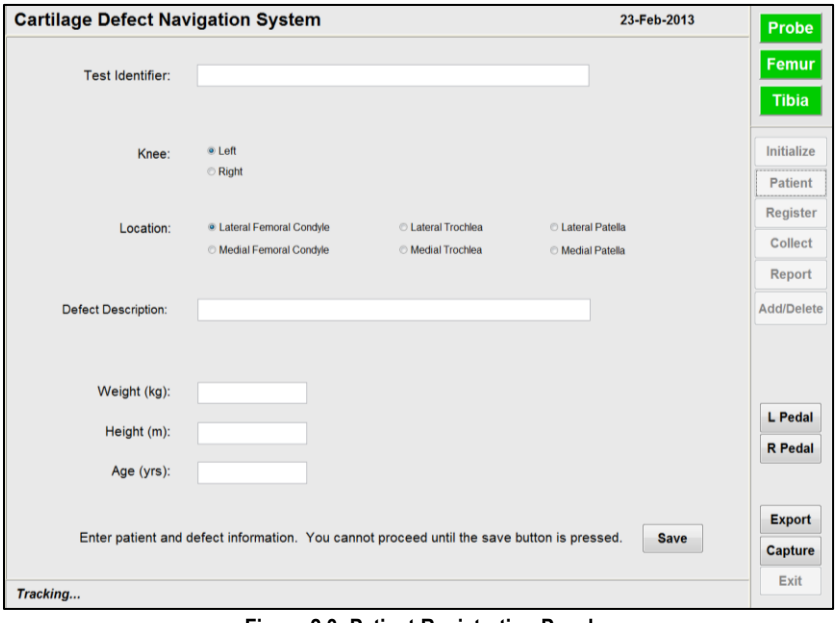

Figure 2.3: Patient Registration Panel

This panel allows surgeons to register information about the patient's defect and patient demographics.

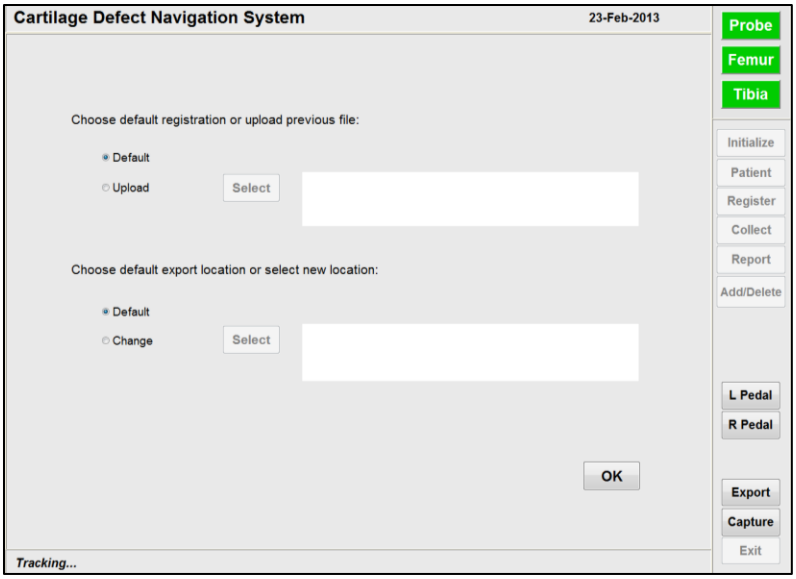

Figure 2.4: Data Save Location Panel
This panel allows surgeons to choose a location to save the data collected from the procedure.

The third step is to attach the optical trackers to the patient. Since this device is intended for arthroscopic procedures the optical trackers cannot be directly attached to the bone, as is used in other surgical navigation systems. To overcome this limitation a percutaneous intraosseous needle (Vidacare EZ-IO, San Antonio) is used for bone fixation. The EZ-IO system utilizes a power driver combined with a 15-gauge needle made from 304 stainless steel to give medical personnel quick access to the intramedullary canal of a bone in military and hospital settings. This system has a special cutting tip, which makes it easy for the needle to penetrate the bone without unnecessary damage to the soft tissue. Once the needle is driven into the bone the power driver attachment is removed leaving a threaded plastic coupling for the optical tracker attachment (Figure 2.5 and Figure 2.6). The EZ-IO system has been shown to provide a firm attachment of the optical trackers to the bone and does not allow for relative motion between the trackers and the patient's bone (Brockmeier, 2009). Upon removal of this EZ-IO needle only a small hole remains in the bone. This hole has been shown to heal in several days and is not believed to present a risk for bone fracture or any weakening of the bone (Ong et al., 2009).

Figure 2.5: EZ-IO needle attachment.
EZ-IO needle attachment in Sawbones knee showing the exposed threaded plastic coupling. Optical trackers are then attached to this coupling

Figure 2.6: Attachment of optical tracker to bone utilizing the EZ-IO system.

After attachment of the optical trackers, the fourth step is to calibrate the system. This system calibration involves three secondary steps. The first is to determine the probe tip offset. The surgical probe being used for this application is the Polaris Passive 4-Marker Probe (Figure 2.7) (NDI, Waterloo, Ontario, Canada). The camera is able to track the location of the four optical tracking spheres attached to this probe, but it is unable to determine the location of the probe tip until this calibration step is performed. To perform this calibration surgeons places the probe tip in a block with a divot cut into it and rotate the probe (Figure 2.8). Once the system has collected enough data points it is able to calculate the probe tip offset using previously established algorithms (Siston et al., 2006).

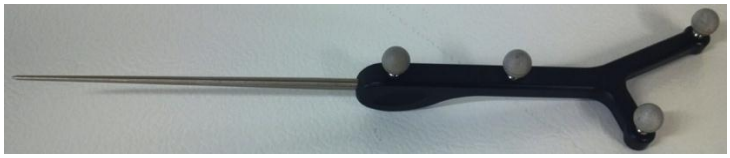

Figure 2.7: Polaris Passive 4-Marker Probe

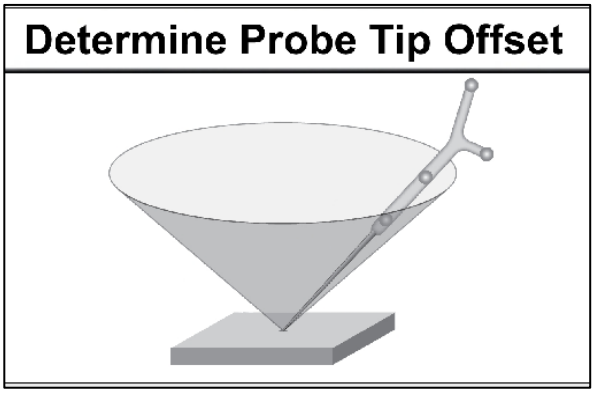

Figure 2.8: Probe tip calibration.
Image showing the rotation motion performed by surgeon to calibrate the probe tip offset. The block with the divot cut into it can be seen at the bottom of the image.

After the probe is calibrated surgeons must determine the three-dimensional location of specific anatomical landmarks on the patient. The first of these landmarks is the hip center or the center of the femoral head. To calculate the hip center surgeons must circumduct the hip while the system tracks the location of the femur (Figure 2.9). The hip center is then calculated using previously established algorithms (Siston et al., 2006). After determining the hip center location, surgeons must manually choose the rest of the essential anatomical landmarks, also known as digitizing landmarks. These landmarks consist of the anterolateral posterior cruciate ligament (PCL) attachment, the medial and lateral epicondyle of the femur, the midpoint of the tibial spines, the medial and lateral contour of the tibia, and the medial and lateral malleolus (Figure 2.10).

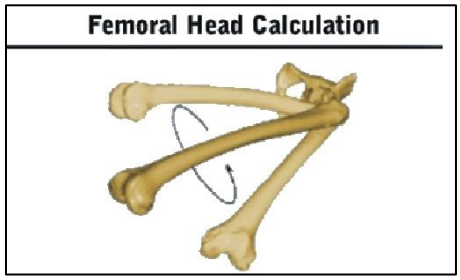

Figure 2.9: Calculating hip center.
Circumduction motion of the femur that must be performed by the surgeon to locate the hip center of the patient.

Figure 2.10: Digitized landmarks.
Specific landmarks that must be digitized by user to generate anatomical coordinate system.

By locating these landmarks the system is able to calculate anatomical coordinate systems (ACSs), which are three-dimensional coordinate systems relative to the patient's femur and to the patient's tibia (Figure 2.11) (Siston et al., 2006; Brockmeier, 2009).

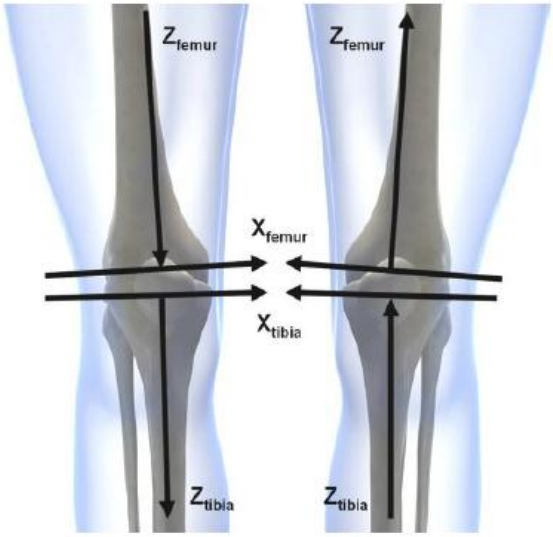

Figure 2.11: Anatomical Coordinate Systems of the Knee
Image courtesy of Brockmeier, 2009.

The origin of the femoral ACS is set as the anterolateral attachment of the PCL. The z-axis of the femur is set as a vector from the hip center to this origin. A temporary vector is then created between the points digitized on the medial and lateral epicondyles and this vector is crossed with the z-axis to generate the y-axis. The z-axis and y-axis are then crossed to generate the x-axis.

The origin of the tibia ACS is set as the midpoint of the tibial spines. The z-axis of this coordinate system is set as a vector from the ankle center to this midpoint, with the ankle center defined as the midpoint of the points digitized on the medial and lateral malleoli (Siston et al., 2005). A temporary vector is formed between the points digitized on the medial and lateral borders of the tibial plateau and is crossed with the z-axis to form the y-axis. The z-axis and y-axis are then crossed to form the x-axis.

For both the ACSs the positive x-axis is oriented from lateral to medial, the positive y-axis is oriented from anterior to posterior, and the positive z-axis is orthogonal to the x-axis and y-axis and based on the cross-product of these two axes. This causes the direction of the positive z-axis to change based on the leg of interest.

Since the optical trackers can be attached to the patient's femur and tibia in any orientation, developing these ACSs is necessary so the results we obtain make anatomical sense. These ACSs allow the navigation system to determine the location of the tibia relative to the femur, which is necessary for the system to calculate the kinematics of the patient, one of the possible data collection functions of the system (Brockmeier, 2009). Also, the axes of the ACSs are used in the approximation of the radius of curvature of the femur in both the frontal plane and the sagittal plane, two of the possible data collection functions of the system (Brockmeier, 2009).

After the system is calibrated, the surgeons are able to begin collecting data about the patient and the patient's defect. When surgeons choose to begin collecting data the data collection panel appears with 5 different options for data collection (Figure 2.12). "Measuring Distance" allows the surgeons to measure the three dimensional distance between any two points in space. "Trace Defect" allows surgeons to trace the boundary of the defect. This boundary tracing is then used to calculate various attributes about the defect, including the area. "Frontal Radius of Curvature" and "Sagittal Radius of Curvature" allow the system to calculate the radius of curvature of the femur in both the frontal plane and sagittal plane, respectively. "Kinematics" allows surgeons to cycle the knee through its full range of motion to determine the

internal/external rotation, varus/valgus angle, and flexion/extension of the patient's knee. While all of these attributes of the system are important to its overall functionality, the focus of this project was on the "Trace Defect" function so the rest of this document will be focused on this portion of the system.

When surgeons decide to begin tracing the defect area they must press the "Trace Defect" button on the data collection panel. When this is done the "Trace Defect" button changes its text to say "Stop" and the other function buttons become deactivated (Figure 2.13).

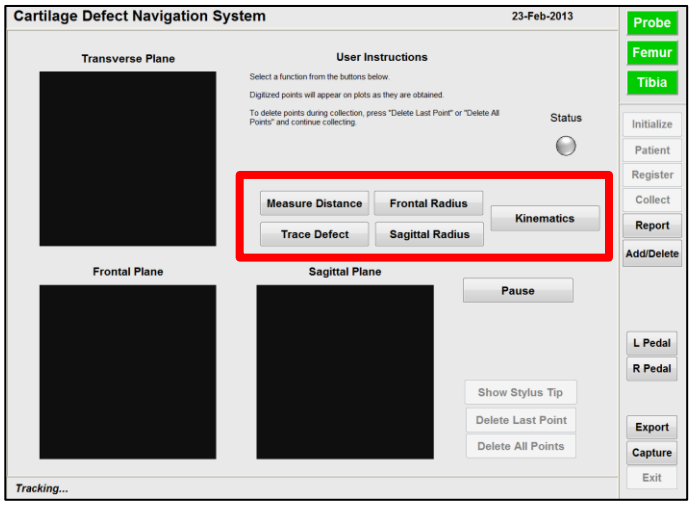

Figure 2.12: Data collection panel.
Outlined in red are the 5 different data collection functions of the system.

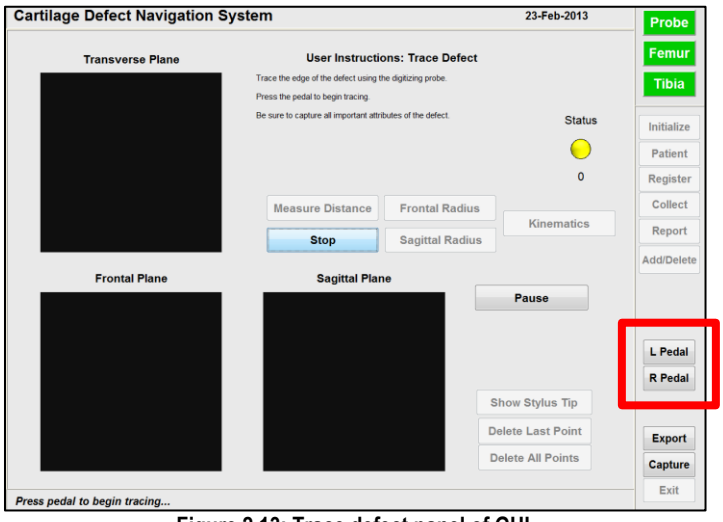

Figure 2.13: Trace defect panel of GUI.
Either pedal button, outlined in red, must be pressed to begin collect data points for tracing.

In order to begin collecting data points around the boundary of the defect surgeons must press either the “L Pedal” button or the “R Pedal” button located on the right hand side of the navigation system panel or the pedal located by the their feet. During arthroscopic procedures there are different pedals at surgeons’ feet to allow them to perform different functions, such as taking photos with the arthroscopic camera. For this system we have the option of allowing surgeons to press a pedal by their feet or to have another member of the surgical team press the pedal button on the user interface.

Either way, once the pedal is activated the system will begin digitizing the three-dimensional location of the probe tip as discrete points. Using the probe tip surgeons are able to trace the boundary of the defect. As they are tracing the defect boundary the three-dimensional location of each point collected will appear on the black plots labeled “Transverse Plane”, “Frontal Plane”, and “Sagittal Plane” (Figure 2.14). These three plots represent the anatomical planes of the body, which were generated from the anatomical coordinate systems relative to the patient’s femur and tibia.

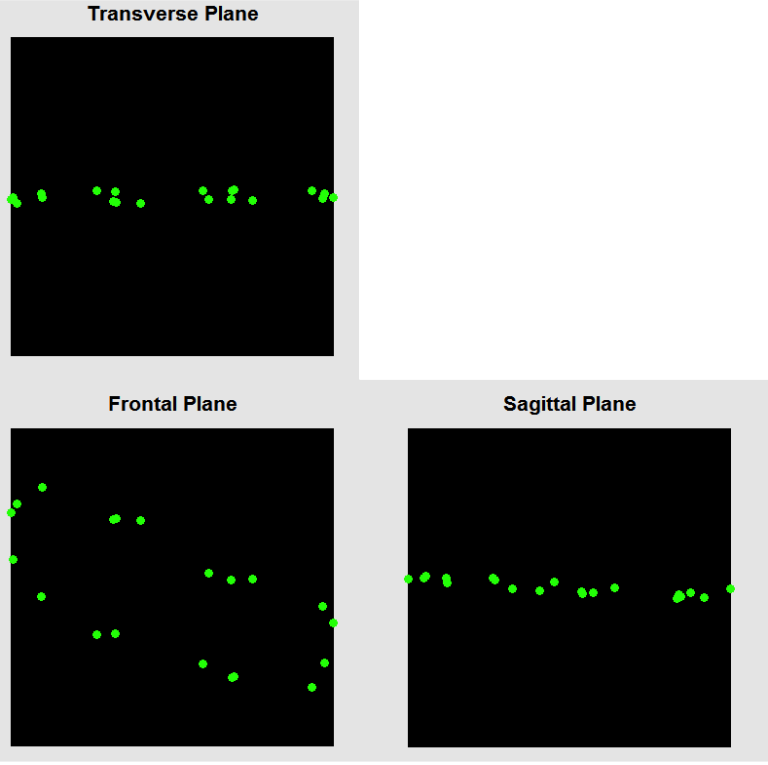

Figure 2.14: Plots showing the three-dimensional location of digitized points.

An additional important feature that increases the usability of the device is the visibility panel in the upper right hand corner (Figure 2.15). This visibility panel tells the user if the camera is able to see the surgeon's probe, the optical tracker attached to the femur, and the optical tracker attached to the tibia. In order for the system to be able to recognize each of these tools at least three of the optical tracking spheres on the tool must visible at any given instant. If the camera is able to see the tool the visibility panel displays this tool as green. However, if the camera is unable to see the tool the visibility panel displays it as red.

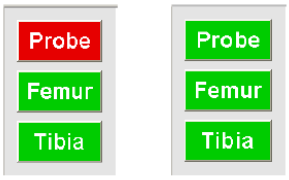

Figure 2.15: Visibility panel.
The visibility panel tells the user if the camera is able to see any of these tools at a given instant. If the tool is visible it is displayed as green and if it is not, it is displayed as red.

After surgeons are finished tracing the defect and feels they have captured all the details of the defect boundary they can press the "Stop" button to end the tracing. To calculate the area of the defect the surgeon must press the "Report" button, located on the right hand side of the data collection panel. When this button is hit the data report panel appears (Figure 2.16). This panel is where all the information collected about the defect is displayed. In the upper left hand corner the statistics about the defect are listed. These include the defect area, the medial-lateral and anterior-posterior width of the defect, the length to width ratio to show the elongation of the defect, and the orientation of the defect relative to the medial-lateral axis of the femoral coordinate system. If the surgeon chooses to collect data on the frontal and sagittal radii of curvature, then these values would also be displayed in the statistics section. Along with the defect statistics this panel also displays three plots. These are for the frontal plane radius of curvature, the sagittal plane radius of curvature, and the defect plot. Since we did not collect any data for the radii of curvature of the defect these plots are currently blank.

The Defect Plot displays a two-dimensional projection of the defect tracing. This two dimensional projection is produced from the three dimensional location of the data points collected. To generate this projection the system calculates the best-fit plane to the data set (Brockmeier, 2009). Each data point is then projected onto this plane to give an approximated shape of the defect, from which the system can calculate the defect area (Brockmeier, 2009).

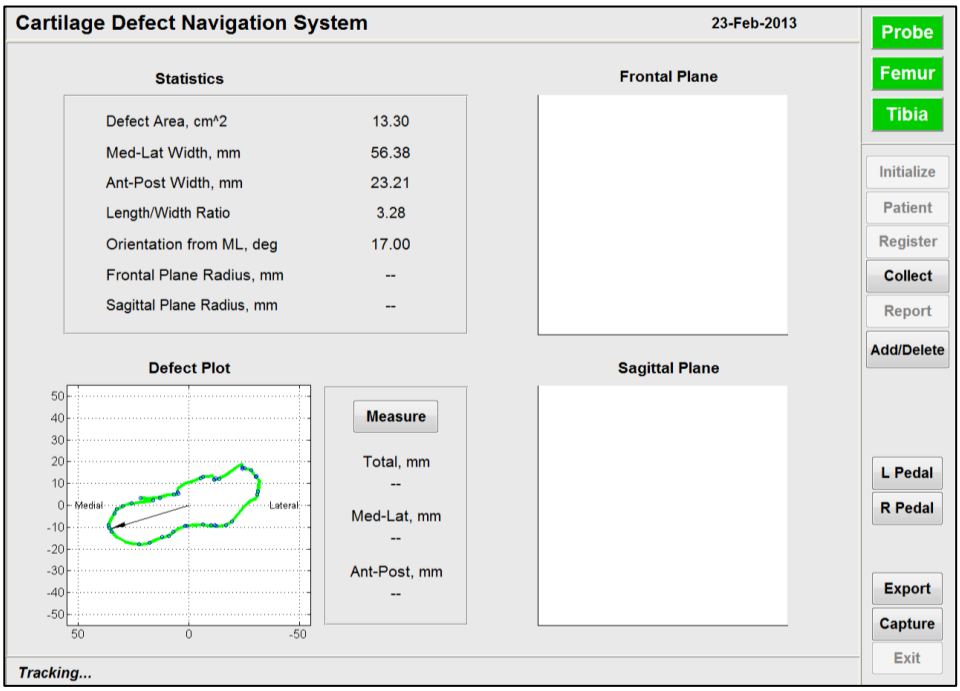

Figure 2.16: Data Report Panel

2.2 Improvements of Previous System

As previously mentioned, the primary goal of this project was to overcome the tracing issues that were encountered with this system when it was tested on defects in cadaver knees. The first of these issues occurred when the surgeons traced around the defect boundary multiple times. To ensure that all the important attributes of the defect were captured the surgeon wanted to trace over the defect boundary multiple times and reverse directions to recollect points in specific areas of the defect. The MATLAB code of the originally developed system used a spline fit that started from the first point collected and ended at the last point collected to approximate the boundary of the defect. The defect area was then calculated

from this boundary using the MATLAB function *polyarea*. However, if the surgeon was tracing around the defect multiple times, the system still performed the spline fit from the first point to the last point. This caused the system to generate a defect boundary approximation that encompassed the defect multiple times, which lead to a very large over approximation in the defect area (Figure 2.17).

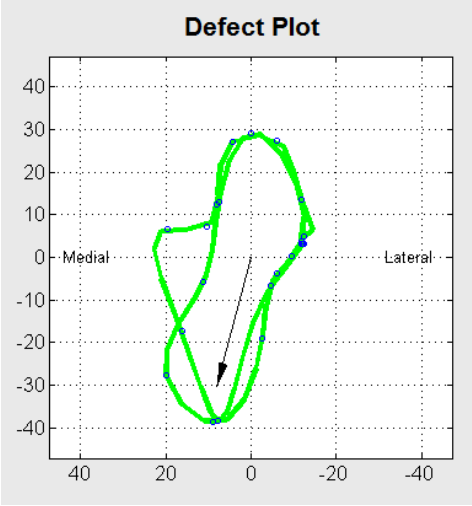

Figure 2.17: Defect boundary generated by previous system
In the previous system, when the defect was traced around multiple times the system calculated the cumulative area of the tracings rather a single area of all the combined points.

A new function was created that is performed prior to the spline fit of the data to overcome this cumulative area calculation. This function, *reorder_points.m*, allows the system to reorder all points collected so that the spline fit only travels once around the defect boundary. The function starts by receiving the two-dimensional location of each collected point relative to the defect coordinate system (Figure 2.18.1). The function then finds the centroid of the data by calculating the average x value and the average y value (Figure 2.18.2). The function then finds the angle of each data point relative to the positive x-axis of the defect coordinate system using the *atan2* function (Figure 2.18.3). After the angle of each point is found, they are put into order from the smallest to the largest angle (Figure 2.18.4). The system then reorders all of the data points with the first point becoming that with the smallest angle and last point being that with the largest angle, relative to the positive x-axis (Figure 2.18.5). After this is performed the spline fit is able to properly function as intended.

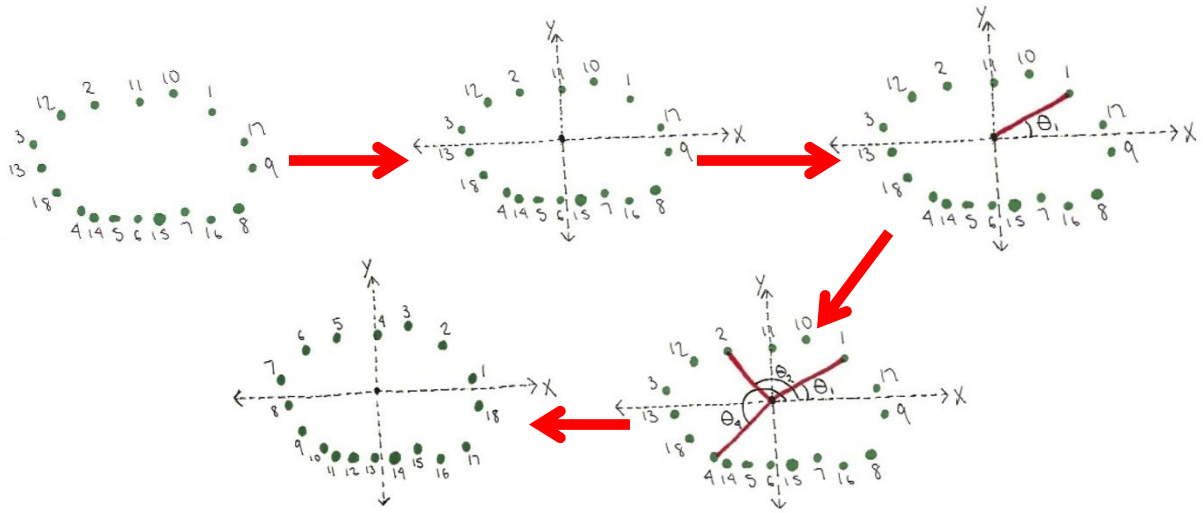

Figure 2.18: Sketch showing the flow of reorder_points.m.

The other major problem encountered by surgeons was caused by the roughness of the subchondral bone and other uncontrollable factors that made it difficult for the surgeons to keep the probe tip on the defect boundary. This roughness caused the surgeon to collect points that were both inside the actual defect boundary and outside the defect boundary. This inaccurate tracing had an impact on the overall defect area calculation, which decreased the area approximation accuracy of the system.

A new panel was created for this system to allow surgeons to choose which points they want to keep in the data set. After surgeons have finished tracing the defect boundary and are done collecting points they have the option to press the “Add/Delete” button located on the right hand side of the data collection panel (Figure 2.19).

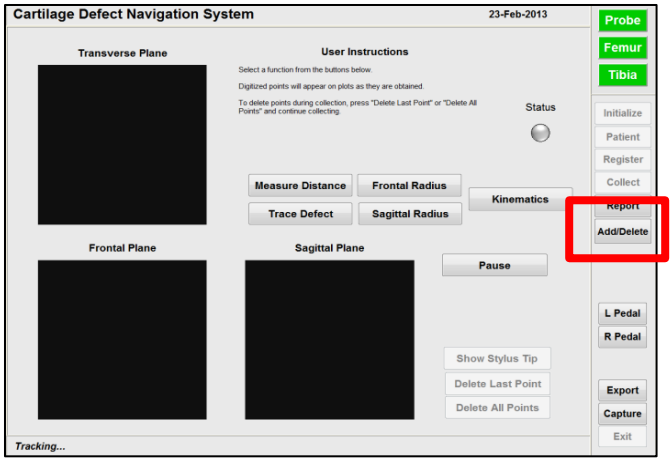

Figure 2.19: Data collection panel with "Add/Delete" button highlighted.

When this button is hit it the GUI displays the modify points panel (Figure 2.20). This panel displays the defect plot, the same one that is displayed in the data report panel, which is a two-dimensional projection of the defect boundary. In this panel the user has three options for functions to use. The first of these functions is to display the stylus tip, also known as the probe tip. When the “Show Stylus” button is selected the text changes to “Stop” and the other two buttons become deactivated. To show the probe tip the surgeon must press either pedal button or the pedal by his feet. When this is done the location of the stylus tip will appear on the defect plot as a red dot (Figure 2.21). This feature is useful in helping the surgeon determine which points should be included in the defect boundary and which points were caused by tracing errors. This function will also allow the surgeon to determine which portions of the defect have accurately been captured by his tracing and which portions need to be modified.

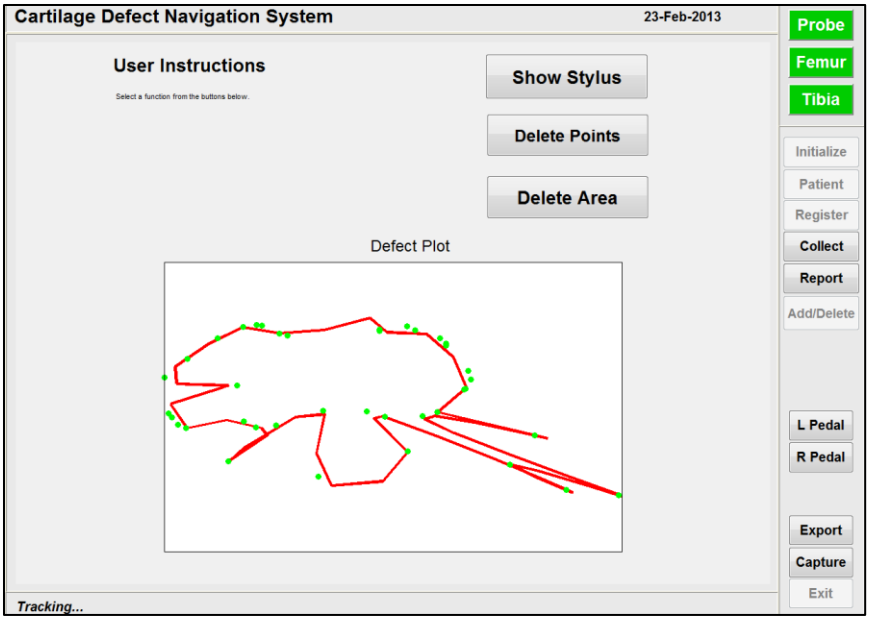

Figure 2.20: Modify points panel.

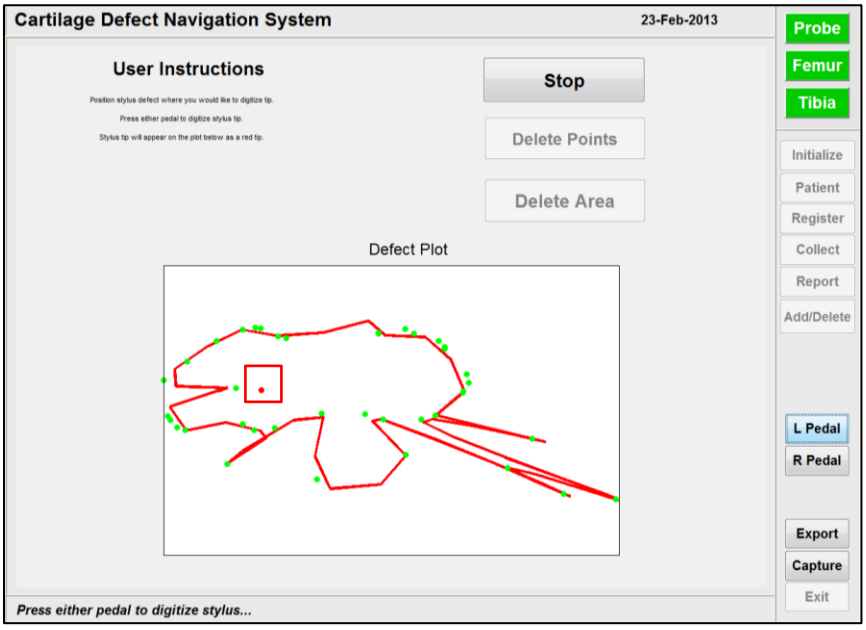

Figure 2.21: Show stylus function in modify points panel.
In this image the stylus tip can be seen as a red dot on the defect plot.

The delete points and delete area functions of this panel allow surgeons to remove the points they have decided were caused by tracing errors. The delete points function gives surgeons the option to remove points one at a time. After surgeons press the “Delete Points” button, they must use the mouse to click on the specific point they want to delete on the plot. The system then determines which point in the data set is closest to the location where the mouse was clicked and removes this point from the data set. A

new spline fit is performed to the modified data set and this spline fit is plotted in the Defect Plot. Surgeons can continue to delete as many points as they feel is necessary.

The delete area function allows surgeons to delete more than one point at a time. After selecting the "Delete Area" button, the surgeons are asked to select four points around the area they would like to remove (Figure 2.22). The points in this selected area are then deleted from the data set. The system then recalculates the spline fit to the modified data set and plots this data set and the spline fit on the defect plot.

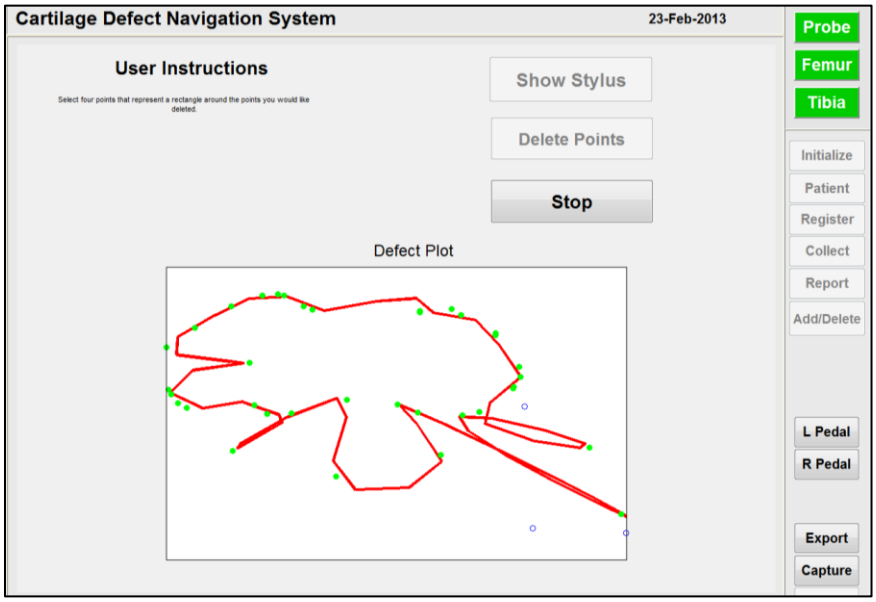

Figure 2.22: Delete area function in modify points panel.
In this image three of the four points the surgeon must select can be seen. When the surgeon selects the fourth point all the points in this area will be deleted.

Surgeons have the option to continually use the delete points and the delete area functions as much as they would like until the defect plot is an accurate approximation of the defect boundary (Figure 2.19). If surgeons decide they want to better define a specific region of the defect or feel they have deleted too many points from the data set they can go back to collect more data points by pressing the "Collect" button, located on the right hand side of the user interface. This will return the system to the data collection panel so the defect can be traced again. This time, when the "Trace Defect" button is pressed a dialog box will appear asking if the surgeon would like to keep the current points. This allows the new points collected to either be added to the current data set or to get rid of all the points and completely start over.

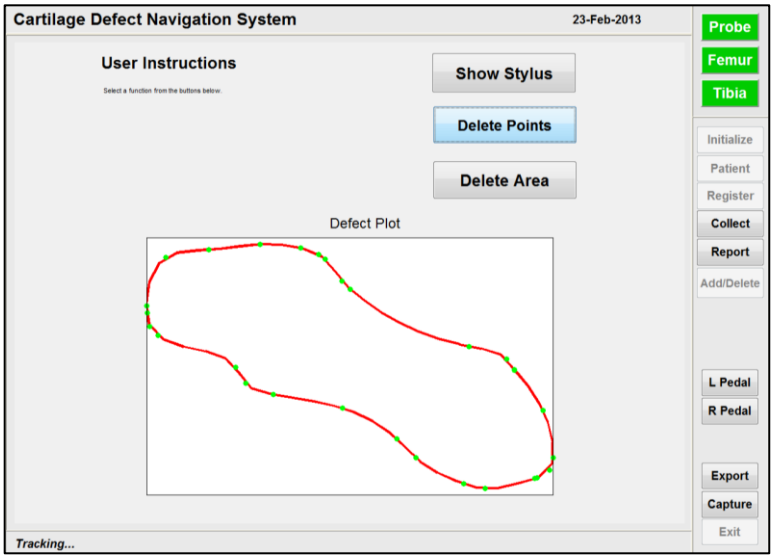

Figure 2.23: Accurate defect boundary approximation.
Defect boundary approximation that was created by deleting points and deleting regions of points that were caused by tracing errors.

2.3 Additional Aspects of System

2.3.1 Navigation System Features

Along with the features of the device created to overcome the previous tracing issues, there were a couple of additional features that were added to increase the usability of the device. The first of these was to allow the system to continuously collect data points. The previously developed system forced the user to select data in a point-by-point method with the pedal being pressed each time surgeons wanted to collect a data point. In the current system, as soon as the pedal is pressed in the trace defect function, frontal radius of curvature function, and the sagittal radius of curvature function the system begins to continuously collect data. This ability allows surgeons to focus more on capturing the desired points rather than worrying about capturing the data points at each instant. Also, this allows surgeons to collect more data points in a given time period, which can help increase the accuracy of the calculations of the system.

Surgeons also have the option to stop collecting data or to pause the data collection at any point during the tracing. This option allows surgeons to move the probe to different portions of the defect without being forced to keep the probe tip on the defect boundary the entire time. Pausing the data collection also gives

surgeons access to three additional system features: "Show Stylus Tip", "Delete Last Point", and "Delete All Points." (Figure 2.24).

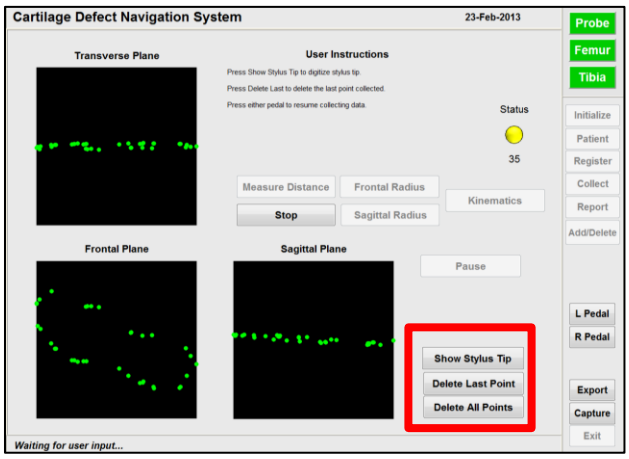

Figure 2.24: Paused status of trace defect function.
When the trace defect function is paused three additional features of the system are made visible, highlighted in red above.

The "Show Stylus Tip" function is the same as the "Show Stylus" function in the previously discussed modify points panel, except this time the three dimensional location of the probe tip is displayed on the three anatomical planes plots (Figure 2.25). This function can help surgeons reorient themselves while collecting data points and help them determine which areas of the defect need to be more fully digitized. "Delete Last Point" allows surgeons to delete the last point that was collected as many times as desired, so it is possible to delete multiple points with this function. "Delete All Points" allows surgeons to get rid of all the data points that were collected and start over with a new tracing.

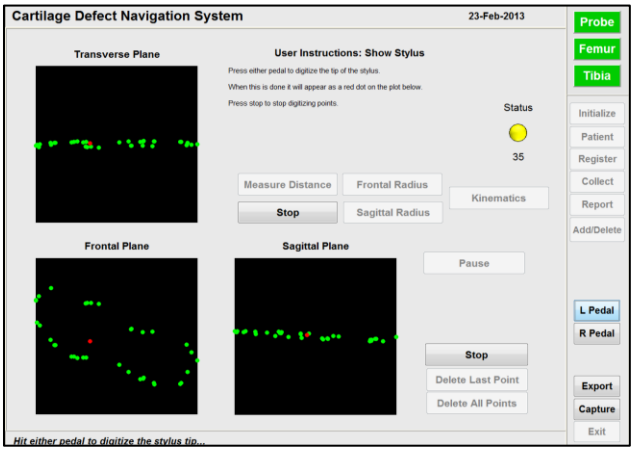

Figure 2.25: Show stylus tip function during defect tracing.
When using the show stylus tip function either one of the pedal buttons can be used to displace the three dimensional location of the stylus tip relative to the previously collected points in the anatomical plane plots.

2.3.2 Hardware

New optical trackers were also developed to improve the accuracy and the usability of the cartilage surgical navigation system. The previous trackers contained three optical tracking spheres in a planar geometry (Figure 2.26). For the tracking camera to recognize a tracker it must be able to see at least three tracking spheres at a time. By having only three spheres in this specific geometry it is much more likely the tracker will rotate out of the camera's plane of view making it more difficult to capture data points while tracing. The new trackers consist of four optical tracking spheres in a three dimensional geometry (Figure 2.27). Having four tracking spheres makes it much less likely that the tracker will move out of view during tracking. Five different trackers were designed and fabricated for this device.

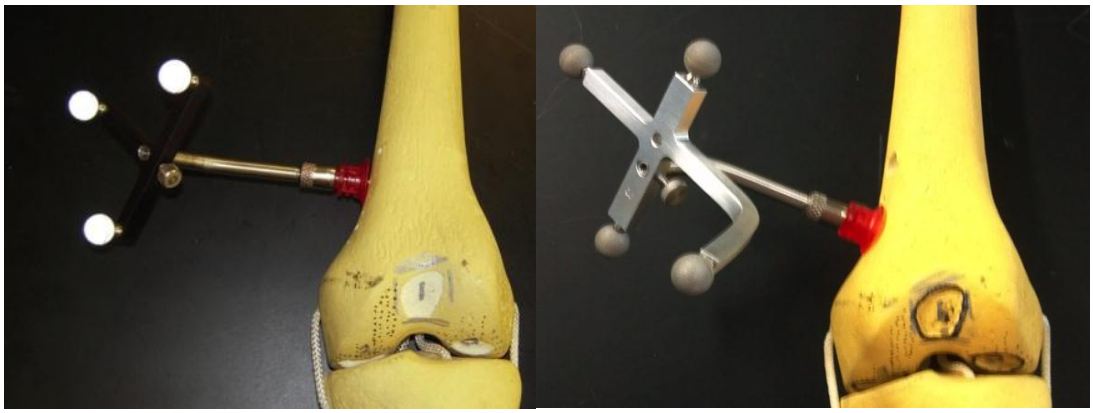

Figure 2.26: Old and new optical trackers.
The trackers in the previous system contained only three optical tracking spheres, whereas the new trackers contain four spheres leading to an increase in the ease-of-use of the device.

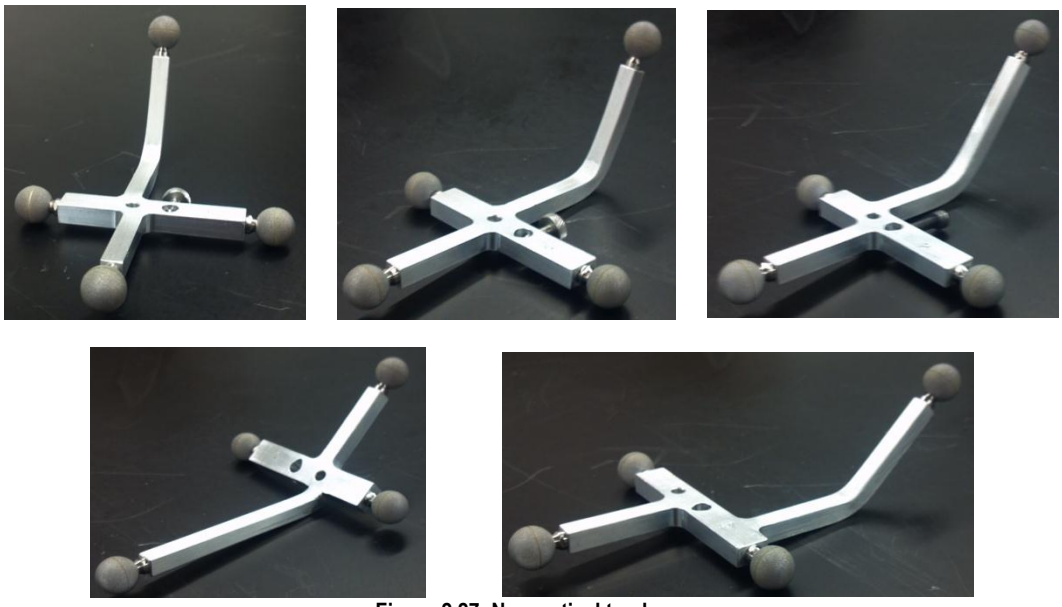

Figure 2.27: New optical trackers.

Chapter 3 : Validation of Navigation System

The motivation for developing this cartilage surgical navigation system was to overcome the inability of surgeons to accurately calculate the cross-sectional area of articular cartilage defects. A validation procedure was set up to compare the use of the navigation system to 3 current manual techniques used by surgeons to determine if this device is able to overcome this weakness. Both the navigation system and the manual techniques were tested on shapes cut into plastic and artificial defects cut into Sawbones knees of known area. Each of these techniques tested were analyzed to determine the accuracy with which each technique predicted the area of the shapes and defects.

3.1 Testing Procedure

This study was an IRB-approved study involving 9 different subjects. These subjects had an average age of 22.8 ± 3.0 years. Each subject was asked to perform four different approximation techniques, three manual and one computer-assisted. Each of these techniques were used to approximate the area of four circles, two ellipses, and three abnormal shapes cut into plastic using a CNC milling process (Figure 3.1) (Brockmeier, 2009). After performing the area approximation on these two dimensional shapes, each of these techniques were used to approximate the area of five artificial defects cut into a Sawbones knee (Figure 3.2) (Brockmeier, 2009).

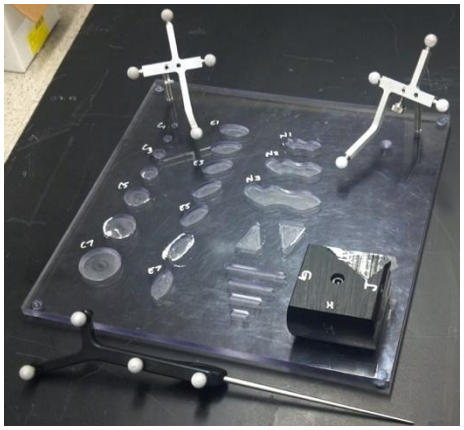

Figure 3.1: Testing set-up for two dimensional shapes area approximation.

Figure 3.2: Artificial defects cut into Sawbones knee.

The three manual techniques used were those that are commonly used by surgeons during a cartilage repair procedure. These manual techniques tested were: (1) Using a ruler, (2) Using an arthroscopic probe with a 5 mm tip, and (3) Using an arthroscopic probe with a retractable tip with markings every 2 mm (Figure 3.3). For each of the manual techniques tested the subjects had three options on how to approximate the area of the shape: (1) State the approximate area (e.g.,"2 cm^2"); (2) State a length and a width to be multiplied together to approximate the area of the defect ("3 cm by 1 cm"); or (3) Approximate the area as a geometric shape and state the dimensions of that shape necessary to calculate the area ("a circle with a 2 cm diameter").

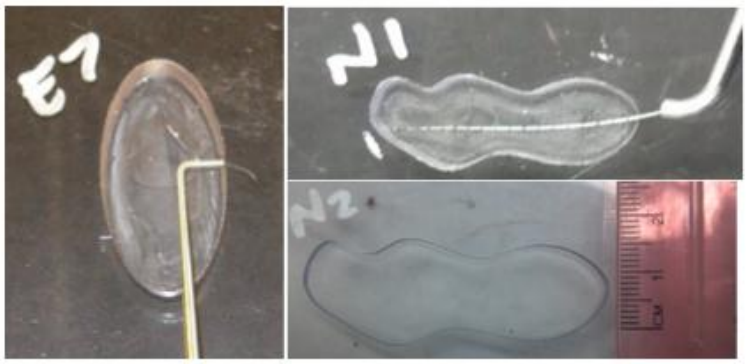

Figure 3.3: Three manual tracing techniques used for system validation.
These techniques consisted of using a 5 mm arthroscopic probe, a retractable arthroscopic probe with 2 mm markings, and a ruler.

The computer-assisted technique was using the surgical navigation system to trace the defect boundary to approximate the area (Figure 3.4). For this portion of the testing subjects were shown how the trace defect function of the system works, how to begin collecting data using the pedal buttons, and how to

pause the system during their tracing. The ability of the system to delete points or modify the points was not introduced to the subjects for this portion of the testing. Each of the subjects was instructed to use the probe tip to trace the boundary of the shape or the defect. There was no instruction on the number of points that should be collected, but rather the subjects were told to collect as many point as they felt was necessary to accurately approximate the boundary of the shape.

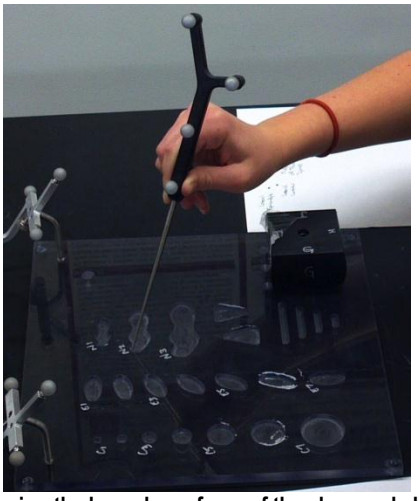

Figure 3.4: Subject tracing the boundary of one of the abnormal shapes during testing.

The subjects were introduced to the ability of the system to delete points while tracing and to modify the data set, after completing the first round of shape tracing. They were given the opportunity to first test these new functions and then were asked to performing the tracing again, but this time they did not have to take as much care to not make mistakes while tracing. After they finished tracing they were allowed to use the modify points panel to remove points from the data set. This portion of shape tracing was only performed with the three abnormal shapes and Sawbones defects numbers 1 and 5.

To obtain a reference for the actual area of each of the shapes cut into plastic a picture of each shape was taken next to a ruler. By using the ruler as a reference line the area of each shape was calculated in Adobe Acrobat Pro X using the area measurement function. For this area measurement function the system is calibrated using the ruler to provide a conversion from pixels to centimeters. The boundary of the shape is then traced and the area of the traced boundary is calculated (Figure 3.5). This calculation was

performed three times and the average of the three tracings was taken to be the actual area of the shape. To determine the actual area of the Sawbones defects molding rubber was pressed into the defect to obtain a mold of the defect shape. The defect shape was then colored in with a silver marker and a picture was taken with a ruler. Using Adobe Acrobat Pro X as before, the area of the defect was approximated by tracing the boundary (Figure 3.6). The actual area was taken as the average of three tracings.

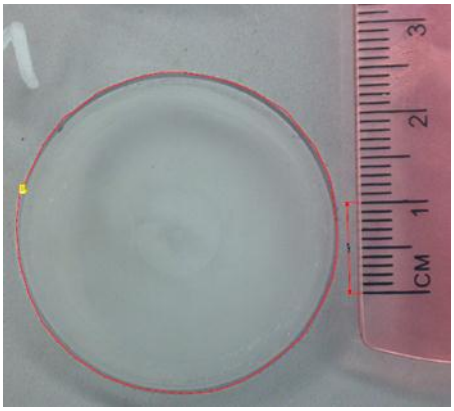

Figure 3.5: Technique used to determine area of plastic shapes.
Using Adobe Acrobat Pro X we were able to trace the boundary of the shape and approximate the area.

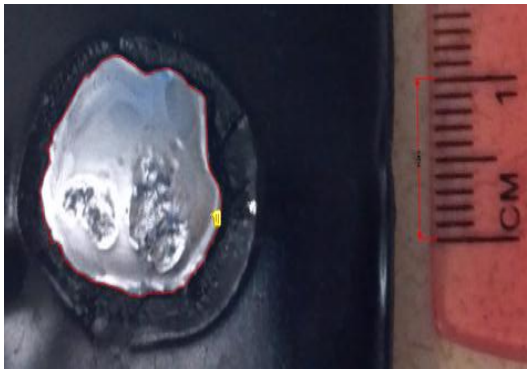

Figure 3.6: Technique used to determine area of Sawbones defects.
Using Adobe Acrobat Pro X we were able to trace the boundary of the defect shape and approximate the area.

The average error and the absolute average percent error were taken for each of the tracing methods. The absolute average was used because some measurements resulted in overestimations (positive values) and some resulted in underestimations (negative values). To prevent a canceling effect from these two opposite errors the absolute average was used. Percent error was chosen to allow for an easier comparison between shapes and defects of varying sizes. The significance between errors in area approximations was compared used a paired student T-test with a Bonferroni correction. When comparing

the navigation system to the 3 manual techniques significance was set at $p < 0.0167$. When comparing the unmodified tracing of the navigation system to the modified tracing and the 3 manual techniques significance was set at $p < 0.0125$. To compare the significance between errors in area approximations a paired student T-test. An acceptable error in the cartilage navigation system was set at 5% error.

3.2 Testing Results

The average area approximation error experienced for all shapes for the ruler, 5 mm probe, retractable probe, and navigation system techniques was -0.055 ± 0.403 cm^2, -0.974 ± 1.42 cm^2, -0.148 ± 0.362 cm^2, and -0.069 ± 0.148 cm^2, respectively. Although comparing these numbers directly does not suggest which is the most accurate, the fact that they are all negative suggests that each technique tends to produce an underestimation of the area. Since the navigation system also had a smaller overall standard deviation it suggests this system is better at producing repeatable measurements, as expected.

The area approximation error for all shapes for the ruler, 5 mm probe, retractable probe, and navigation system techniques was 15.4 ± 12.9%, 23.6 ± 8.0%, 16.2 ± 10.8%, and 10.7 ± 9.5%, respectively (Figure 3.7). The overall error generated by using the cartilage navigation system was significantly less than that produced by using the 5 mm probe ($p = 0.004$) but it was not significantly less than using the retractable probe ($p = 0.017$) or the ruler ($p = 0.058$).

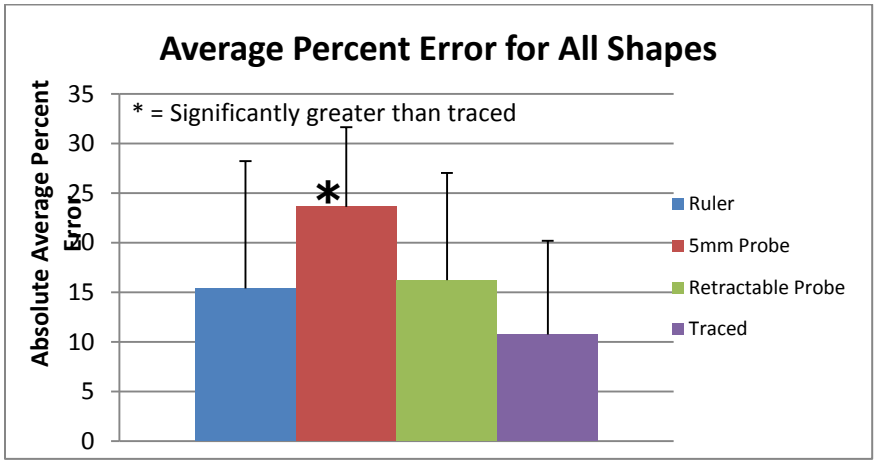

Figure 3.7: Absolute average percent error for each tracing technique for all shapes.
Error bars represent one standard deviation from the mean.

The error associated with using the cartilage navigation system to measure the normal shapes (the perfect circles and the perfect ellipses) was 8.08 ± 7.09%. This was not significantly less than the errors associated with using a ruler, 6.35 ± 6.94% ($p = 0.476$), a 5 mm probe, 19.8 ± 4.96% ($p = 0.034$), or a retractable probe, 8.93 ± 3.87% ($p = 0.716$) (Figure 3.8).

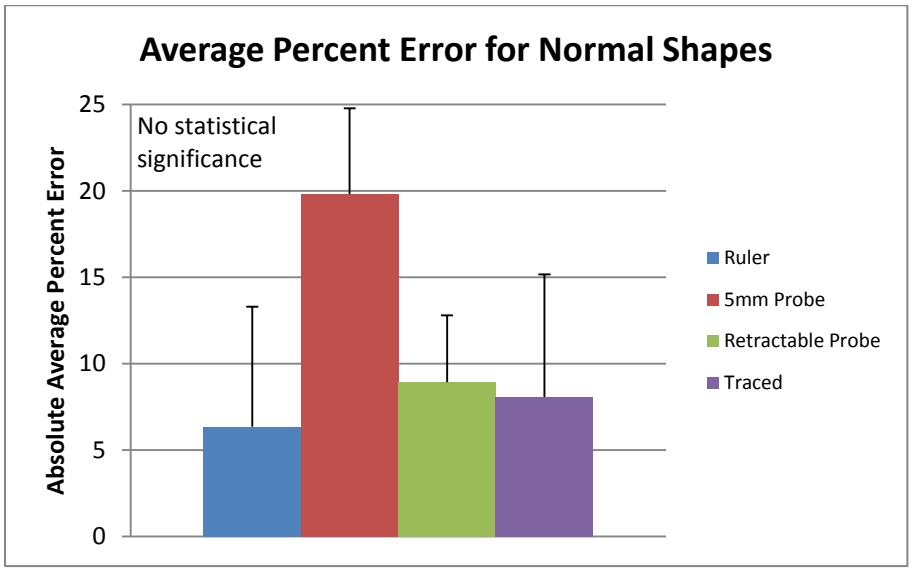

Figure 3.8: Absolute average percent error for normal shapes.

When approximating the area of the abnormal shapes the cartilage navigation system only experienced an average error of 5.80 ± 1.54%. This was significantly less than the errors that occurred when using a ruler, 16.0 ± 2.49% and a 5 mm probe, 36.6 ± 3.75% ($p = 0.005$ and $p = 0.007$, respectively), but it was not significantly less than using a retractable probe 20.0 ± 3.66% ($p = 0.037$) (Figure 3.9). This is important when relating these results back to cartilage defects because typically defects are abnormal shapes and are very rarely close to normal geometric shapes. When users were given the freedom to begin deleting points from the tracing the error in the area approximations actually increased to 11.3 ± 3.40%, which was not a significant amount ($p = 0.039$) (Figure 3.10).

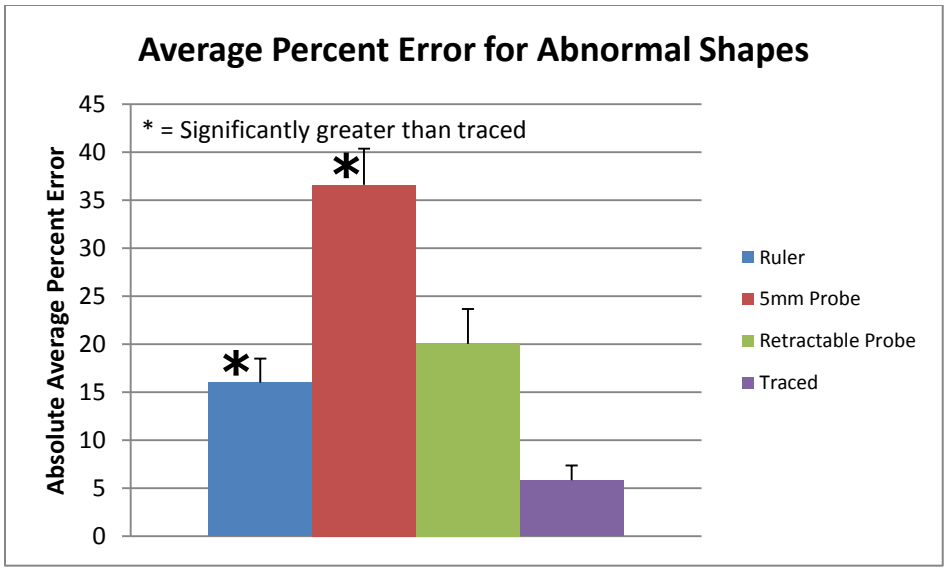

Figure 3.9: Average percent error for abnormal shapes.

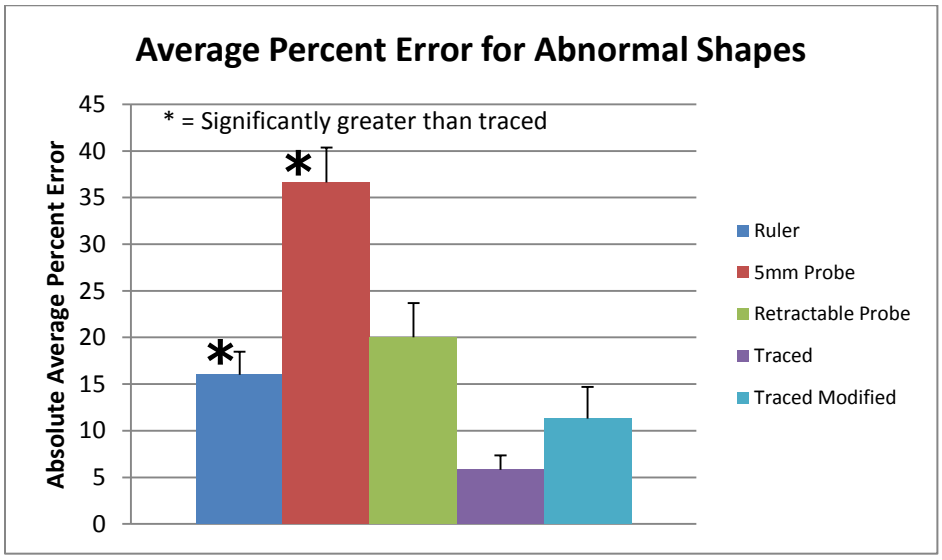

Figure 3.10: Absolute average percent error for abnormal shapes with modified tracing.

When approximating the area of the artificial defects made in Sawbones knees the cartilage navigation system performed the best with an error of 16.9 ± 12.3%, but it was not significantly better than the other techniques. The techniques using a ruler, a 5mm probe, and a retractable probe produced errors of 25.8 ± 14.7% ($p = 0.091$), 20.4 ± 3.18% ($p = 0.523$), and 22.8 ± 14.5% ($p = 0.130$), respectively (Figure 3.11). When the subjects were allowed to modify their points after tracing the error of the navigation system decreased to 9.99 ± 4.67%, but we were unable to determine the significance of this value because only two of the Sawbones defects were tested with this method (Figure 3.12).

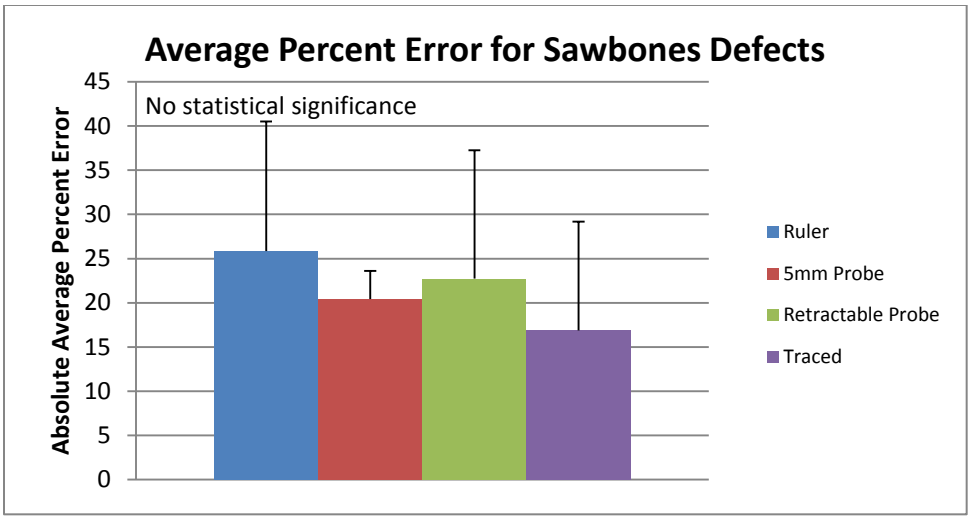

Figure 3.11: Absolute average percent error for Sawbones defects.

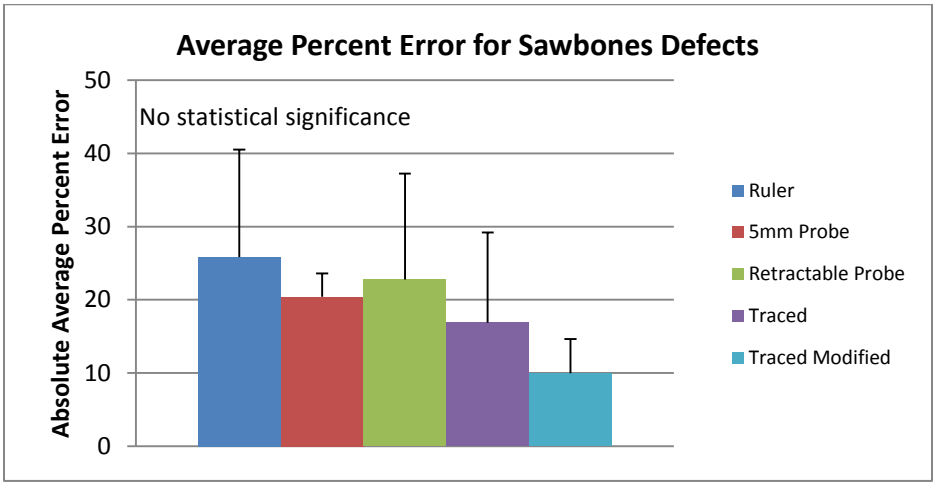

Figure 3.12: Absolute average percent error with modify tracing included.

3.3 Discussion

An acceptable area estimation error was set at 5% prior to beginning validation. The system was not able to reach this threshold for the overall error of all shapes, nor was it able to reach this threshold when the various shapes were separated into subcategories. Since we were unable to reach the desired system accuracy we sought to understand where the increase in the system error was occurring to improve this in future system updates.

The largest amount of error in the system was seen in approximating the area of the Sawbones defects, which is also the most applicable to actual applications of this system. One major cause of this

error is caused by the system's two dimensional approximation of what is actually a three dimensional surface. To determine the amount of error induced by this approximation we performed a comparison of the area of a portion of a cylinder to the project area of the cylinder (Figure 3.13).

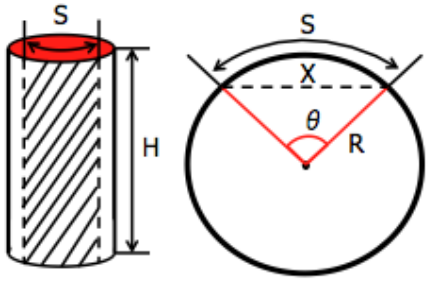

Figure 3.13: Surface area of a cylinder approximation.
This figure seen here was used to determine the amount of error induced by taking a two dimensional area approximation of a three dimensional defect.

In this figure the area being approximated is the sketched in area of the cylinder surface. The actual area of this surface is equal to:

$$Actual\ Area = SH \quad (1)$$

By plugging in the equation for the arc length of a portion of a circle into equation 1 we obtain the equation:

$$Actual\ Area = R\theta H \quad (2)$$

Where R is the radius of curvature of the surface and θ is the angle that the surface covers. Based on this same figure the projected area of this surface would be equal to:

$$Projected\ Area = XH \quad (3)$$

Where X is the width of the surface. In order to relate X to θ and to R we can use the fact that:

$$X = 2Rsin\left(\theta/_2\right) \quad (4)$$

By plugging equation 4 into equation 3 we can determine that the projected area is:

$$Projected\ Area = 2RHsin\left(\theta/_2\right) \quad (5)$$

To determine the error induced by this approximation we used the percent area calculation:

$$\% \, Error = \frac{|Actual\ Area - Project\ Area|}{Actual\ Area} \quad (6)$$

Plugging equation 2 and equation 5 into equation 6 and simplifying we obtain:

$$\% \, Error = \frac{\theta - 2sin\left(\theta/_2\right)}{\theta} \quad (7)$$

This shows that the percent error is only a function of the angle the surface, or the defect, covers. However, this attribute of the defect is a value that the cartilage navigation system is unable to quickly calculate. To relate θ back to other attributes that the system can easily calculate we manipulated equation 4 to obtain:

$$\theta = 2\sin^{-1}\left(X/_{2R}\right) \quad (8)$$

Plugging equation 8 into equation 7 we obtain:

$$\% \, Error = \frac{\sin^{-1}\left(X/_{2R}\right) - X/_{2R}}{\sin^{-1}\left(X/_{2R}\right)} \quad (9)$$

This gives us a relationship between the percent area induced by the two dimensional approximation and the ratio of the surface width (X) to the radius of curvature of the surface. By plotting this relationship we see that the error approximation increases at an increasing rate as this ratio, $X/_R$, becomes larger (Figure 3.14). By setting an acceptable level of error at 5% we see that at $X/_R$ approximately equal to one the error begins to exceed this threshold and then rapidly increases from there. Based on this result, when the width of the defect in a specific direction is approximately equal to the radius of curvature of the defect in that same direction then the error in this approximation starts to become pretty large.

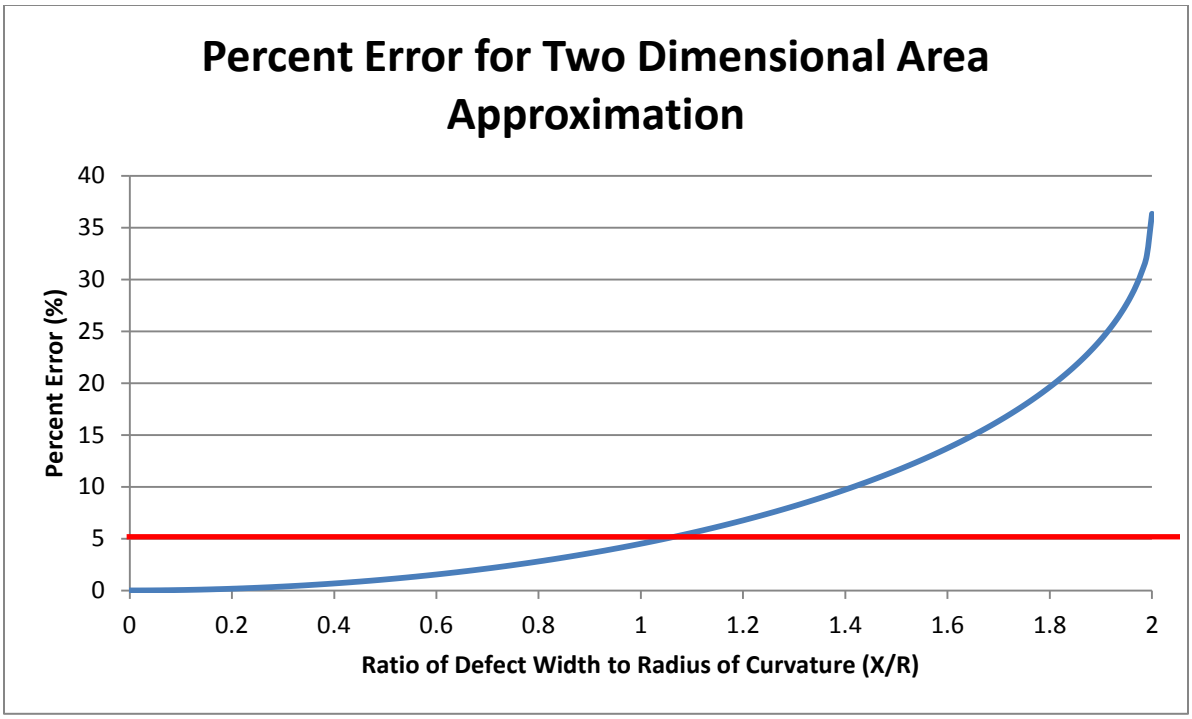

Figure 3.14: Percent error induced by two dimensional area approximation of defect.

For the average femur this approximation is not of much concern. The average femur has a relatively large radius of curvature in each direction, with a minimum radius of curvature of 2.1 cm (Table 3.1). This means that if a defect in the medial compartment of the femur had a width of 2.1 cm in the medial-lateral direction, then this area approximation would be of concern. However, a defect of this size is already a fairly large defect so surgeons would most likely use the more advanced techniques, such as autologous chondrocyte implantation.

Table 3.1: Radii of curvature of average femur.

	Medial Compartment	Lateral Compartment
Medial-Lateral Radius of Curvature (cm)	2.1	2.5
Anterior-Posterior Radius of Curvature (cm)	3.4	2.2

In relating this back to the error of the cartilage navigation system, after measuring the radius of curvature of the femur of the Sawbones knee it was realized that the Sawbones knee is actually smaller than an average knee. This means the radius of curvature of the Sawbones knee is smaller than that of the average femur (Table 3.2). Since the Sawbones femur has a smaller radius of curvature the error in measuring the artificial defects in this study is larger than it would be for measuring these same size defects on an average size femur.

Table 3.2: Approximate radius of curvature of Sawbones femur.

	Medial Compartment	**Lateral Compartment**
Medial-Lateral Radius of Curvature (cm)	1.87	1.72
Anterior-Posterior Radius of Curvature (cm)	2.17	2.0

We determined the error induced in the area approximation of each of the Sawbones defects by measuring the width of each defect in the medial-lateral direction and the anterior-posterior direction. The ratio of the defect width to the radius of curvature of the Sawbones femur $\left({}^{X}/_{R}\right)$ was determined using these measured widths and the values in Table 3.2. By using equation 9 we were able to determine the percent error induced in each area approximation. For each defect we obtained two error values, one in the medial-lateral direction and one in the anterior-posterior direction. The actual error for each defect was taken as the higher of these two errors. We averaged these errors together to obtain an average radius of curvature error of 3.90 ± 1.89%. The total error of the Sawbones defects area approximations using the navigation system was 16.9 ± 12.3%, which is much larger than the error induced by the curvature of the femur. This radius of curvature error is able to explain part of the overall error, but not all of it.

Another possible source of this system error was that when collecting points along the boundary of the defect most users were not collecting enough data points to accurately approximate the defect

boundary. If users do not collect enough data points then the boundary of the tracing will not be an actual approximation of the defect boundary, which in turn will lead to an inaccurate area approximation (Figure 3.15).

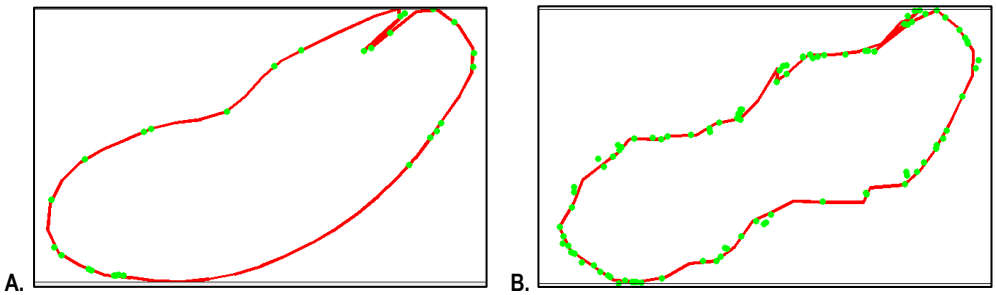

Figure 3.15: Comparison of tracings with different number of data points.
This image compares the same shape traced with a different number of data points. Even though these are supposed to be the same area, image A would lead to an over approximation with less data points collected, whereas image B would produce a better area approximation.

The final probable source of error occurred when subjects were given the option to delete points from their data tracing. When subjects were given this option it appeared that they were more interested in making the defect tracing have smooth edges and curves rather than making the tracing look as much like the actual defect area as possible. This means that they would delete points that, while they appeared to be a portion of the actual defect boundary, made the boundary look rough. By doing this they were actually making the area approximation worse through their point modifications, rather than improving the approximation.

Modifications can be made to the functionality and the use of the navigation system to overcome these errors. An integration technique can be used to more accurately capture the entire area of the defect to minimize the error induced by using a projected area of the defect rather than the actual three-dimensional area. This means that instead of taking a single projection of the overall shape, this projection could be broken into smaller incremental projections. This means the entire three dimensional area of the defect will be broken into a large number of smaller two dimensional areas. By summing together all of these two dimensional areas we can better approximate the three dimensional area of the defect.

Two modifications can be made to overcome the issue of not collecting enough data points to accurately approximate the defect boundary. The first modification can be to set a minimum number of points the user must collect before they can approximate the defect area. More points collected on the defect boundary leads to a more accurate approximation of the defect boundary and an easier ability for users to distinguish outliers in the data set when collecting points (Figure 3.16). By increasing the number of data points collected it becomes obvious which points should be included in the data set and which points were caused by tracing errors. Increasing the number of data points also allows the system to better capture intricate, fine details of the defect.

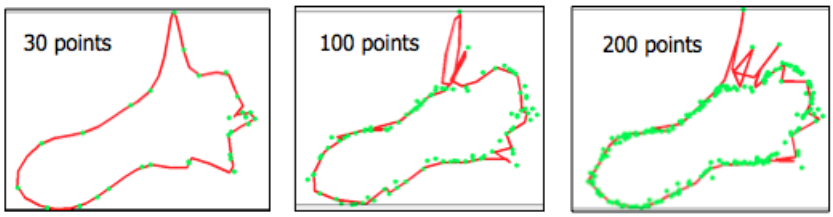

Figure 3.16: Increase in approximation accuracy with more points collected.
By collecting more data points along the defect boundary it becomes easier to approximate the area of the defect and easier to determine outliers in the defect tracing.

The second modification will be to stress to users the importance of capturing all attributes of the defect boundary. During the system testing users were told to use enough points to accurately capture defect boundary, but there was no stress placed on this since part of the study was focused on understanding how subjects used the system. Explaining to future users of the system how important it is that they accurately capture all aspects of the defect will help them to focus more on making their tracing look like the actual defect boundary.

Allowing users to have more practice with the system prior to using it in actual tests or procedures will help overcome the issue of users not properly utilizing the ability of the system to modify points . Showing users how important it is to only delete points that do not fall on the defect boundary and giving them practice in distinguishing outliers will help them increase their understanding of how the system works.

Increasing user familiarity with the system will allow users to produce very accurate approximations of the defect boundary.

Along with these changes there were a few other minor modifications that could help improve the cartilage navigation system. The first of these is to add an “Undo” button to the modify points panel. By adding this feature users will be able to delete points from the system and then determine if they feel they were good points to delete. If not they have the option to undo their selections to bring the points back into the data set. Currently the system allows users to collect more new points after they have deleted points from the data set, but the undo feature is a much faster method of regenerating a couple points the user wants to bring back.

The other modification would be to increase the number of points used in the spline fit of the data. Currently the system performs an interpolation of all the selected data points and chooses 50 data points to generate the spline fit that represents the defect boundary approximation. This is done to decrease the computation time it takes to perform the spline fit. However, during testing it appeared that by limiting the number of points to 50 the accuracy of the spline fit was decreasing with more complex defect shapes. Even though it will increase the computation time, including all of the collected data points in the area approximation will help generate less error in the approximation. It is unknown if this change will have a major impact on the computation time, but we believe the negative of this increased computation time will be outweighed by the benefit of a better area approximation.

The fact that the surgical navigation system performed significantly better in approximating the area of the abnormal shapes than the other techniques is very promising. In actual patients the cartilage defects are typically amorphous structures. This makes it very difficult for surgeons to approximate their area simply from using the area of normal geometric shapes to form this approximation. This suggests that in arthroscopic applications this system will perform significantly better than current techniques at approximating the defect area.

Although the cartilage navigation system did not perform below the overall error threshold of 5% error we believe this will perform even better relative to the manual techniques during arthroscopic procedures performed in cadaver knees and on actual subjects. As previously mentioned, errors in area approximation in manual techniques range between overestimations of 236.61% to underestimations of -78.81% (Siston et al., 2013). Errors of this magnitude were not seen for the manual techniques in this study. This means that the difficulty to manually approximate defect area in actual arthroscopic procedures greatly increases in comparison to approximating the areas in this study. When transitioning from using the previously developed cartilage navigation system in a study similar to this one to use in cadaver knees the additional issues encountered with the system were related to errors in tracing of the defects. Since the new aspects of the cartilage navigation system will allow surgeons to overcome these tracing issues we believe the error in the area approximations will not increase much when using this system in actual arthroscopic procedures. This means the cartilage navigation system will perform even better than the current manual techniques in a normal surgical setting. Even though we believe this difference between manual techniques and the navigation system will be significant we still want to decrease the system error to below 5% before moving forward.

Chapter 4 : Conclusion

4.1 Contributions

The purpose of this project was to improve the previously developed cartilage navigation system and validate the ability of this system to accurately calculate the area of articular cartilage defects. The previously developed system had two major errors that occurred during cadaver testing, both related to unexpected issues in the tracing of the defect boundary. Additional features added to the system have allowed it to overcome these issues. Through reordering of the data points prior to performing the spline fit, surgeons have the freedom to trace the defect boundary as many times as desired and to trace different portions of the defect as much as desired. Through the ability to delete points from the data set surgeons have the freedom to delete outliers in the tracing that occurred due to the probe tip coming off the defect boundary.

This project was motivated by the inability of surgeons to accurately calculate the area of articular cartilage defects using the current manual techniques. Use of the cartilage navigation system has shown to produce an increase in area approximation accuracy. This system is able to be initialized, calibrated, and used to approximate the area of a defect fairly quickly and will not lead to a significant increase in surgery time for a patient, especially by allowing surgeons to practice with the system prior to its use in surgical procedures.

Along with the ability of the system to calculate the area of a cartilage defect this system also has the ability to calculate other attributes of the defect and of the patient. These consist of the ability to measure various distances, to determine the orientation of the defect, to determine the frontal and sagittal radii of curvature of the defect, and to determine the passive kinematics of the patient (Brockemeier, 2009). These attributes will be important for future work investigating other factors that impact the outcomes of patients undergoing articular cartilage defect repair.

4.2 Additional Applications and Future Work

The next step in moving towards application of this cartilage navigation system in actual arthroscopic repair procedures is to make the second round of updates to this system outlined in the Discussion section of this document.. These updates are essential to increase the usability and will increase the accuracy of the defect area approximations of the current device. After these modifications have been performed we will perform the same system validation experiment again to ensure the system is able to predict the defect area within the 5% error threshold. Once this is done we will validate the system on cartilage defects on cadaver knees with the same threshold of 5% error set as our success criteria. After completing this validation we will be able to take this system into the operating room to be used in actual articular cartilage procedures.

Along with helping surgeons accurately calculate the area of a cartilage defect we can also use this device to investigate the relationship between defect size and articular cartilage repair success. For this study surgeons will be given the cartilage navigation system to determine the actual area of the defect, but we will not tell them this area. Instead we will have them perform the surgery as they normally would, without the use of the navigation system, using the currently accepted manual techniques to approximate the area of the defect and to choose the specific procedure for the patient. After following the patient for six months we will be able to determine the surgery success of each patient. By comparing this information back to the defect area calculation performed with the cartilage navigation system we will be able to split this patient group into four sub-populations: (1) Successful surgery and correct procedure; (2) Successful surgery and incorrect procedure; (3) Unsuccessful surgery and correct procedure; (4) Unsuccessful surgery and incorrect procedure. For this study we will define the correct procedure as the procedure that would be chosen if the surgeon knew the actual area of the defect, based on the algorithm that uses defect size as the most important defect attribute. The actual area will be defined as the area the navigation system calculated. If the majority of patients fall are in categories 1 and 4 this suggests that defect size is the most

important factor in determining which procedure to use for each patient. However, if there is an equal distribution of patients between the 4 categories this suggests there are other factors that should be taken into account when choosing a procedure to treat a patient's cartilage defect. These results would provide support for previous studies investigating the impact of defect orientation, location, and shape on subchondral bone contact (Pena, 2007;Brockmeier, 2009;Flanigan, 2010).

These previous studies investigating the impact of various defect attributes on the subchondral bone contact are limited in that they were performed on bovine knees or as finite element studies. This cartilage navigation system provides the ability to perform studies similar to these, but in human knees. By using the ability of the system to calculate these defect attributes during a cartilage procedure we can investigate the relationship between each of these attributes, surgery choice, and surgery success.

4.3 Summary

This research presents the improvement and validation of a cartilage navigation system to be used to determine the cross-sectional area of an articular cartilage defect during an arthroscopic repair procedure. This project made improvements on a previously developed cartilage navigation device both through creating new system capabilities to overcome the tracing issues experienced during tracing of defects in cadaver and through developing new functions to increase the ease-of-use of this system. Through validation of this system, it was proven that use of this device is more accurate than the manual techniques currently used. While the accuracy of the system is above the desired threshold of 5% error, further modifications can be made to the system to further reduce this error. Reduction of this error will allow this device to be used by surgeons to quickly and accurately calculate the area of a cartilage defect during an arthroscopic examination.

The overall goal of this project was to improve the outcome for patients receiving surgery to repair an articular cartilage defect. Current surgical algorithms use the defect size as the most important defect

attribute in determining which specific procedure to use for each patient (Cain et al., 2001; Scott, 2005; Alford and Cole, 2005; Clark et al. 2005; Farr et al. 2004; Scopp and Mandelbaum, 2004). By giving surgeons the ability to determine the actual area of the defect they will be able to make a more informed decision on which specific surgical technique to use for each patient. This theoretically will lead to better functional outcomes for each patient, if the current surgical algorithm using defect area as the most important attribute is correct.

References

Alford J and Cole B (2005). Cartilage restoration, Part 2. Techniques, outcomes, and future directions, *American Journal of Sports Medicine*. 33(3), 443-460.

Andrades JA, Claros S, Jiménez-Palomo P, López Puertas JM, Zamora Navas P, Guerado E, Monleón M, Araque MC, and Becerra J (2011). Skeletal Regeneration by Mesenchymal Stem Cells: What Else?, *Regenerative Medicine and Tissue Engineering - Cells and Biomaterials*, Daniel Eberli (Ed.), ISBN: 978-953-307-663-8, InTech, DOI: 10.5772/20889.

Aroen A, Loken S, Heir S, Alvik E, Ekeland A, Granlund O, et al. (2002). Articular cartilage lesions in 993 consecutive knee arthroscopies. *Arthroscopy: The Journal of Arthroscopic and Related Surgery*. 18(17):730-4.

Brockmeier PM. Surgical Navigation for Articular Cartilage Repair: Motivation, Development, and Validation [Master's Thesis]. Columbus: The Ohio State University; 2009.

Brockmeier P, Harris J, Flanigan D, Siston R. Is 2cm^2 the Correct Threshold Size to Dictate Articular Cartilage Repair? Transactions of the 55th Annual Meeting of the Orthopaedic Research Society, Las Vegas. 2009:1092.

Buckwalter JA, Mow VC, Mankin HJ (2002). Articular cartilage: Structure, function, metabolism, injury and pathogenesis of osteoarthritis. In: The Adult Knee, JJ Callaghan, AG Rosenberg, HE Rubash, PT Simonian, TA Wickiewicz (eds), Lippincott Williams & Wilkens Publishers, Vol 1, Sec 2, 225-236.

Cain EL, Clancy WG (2001). Treatment Algorithm for Osteochondral Injuries of the Knee. *Clinics in Sports Medicine.* April;20(2):321-42.

Clarke H, Cushner F, and Scott W (2005). Clinical algorithm for treatment of chondral injuries, Insall & Scott: Surgery of the Knee, 4th Edition, Volume 1(Chapter 27), 433-437.

Cole B, Pascual-Garrido C, and Grumet R (2009). Surgical Management of Articular Cartilage Defects in the Knee. *JBJS, American.* 91(7), 1778-1990.

Curl WW, Krome J, Gordon ES, Rushing J, Smith BP, and Poehling GG (1997). Cartilage injuries: a review of 31,516 knee arthroscopies. *Arthroscopy.* 13(4):456–460.

Diaz, R., and J. Albright (2008). In search of a gold standard of knee cartilage defect topographical documentation: "freehand" arthroscopic mapping and introduction of new concepts. *Sports Medicine and Arthroscopy Review.* 16(2), 97-102.

Dieppe P (1999). Subchondral bone should be the main target for the treatment of pain and disease progression in osteoarthritis. *Osteoarthritis Cartilage*. 7(3): p. 325-6.

Drawer S, Fuller C (2001). Propensity for osteoarthritis and lower limb joint pain in retired professional soccer players. British Journal of Sports Medicine. 33(3):443-60.

Farr J, Lewis P, and Cole B (2004). Patient evaluation and surgical decision making. *Journal of Knee Surgery*. 17, 219-228.

Fisher NM, Pendergast DR, Gresham GE, and Calkins E (1991). Muscle rehabilitation: its effect on muscular and functional performance of patients with knee osteoarthritis. *Arch Phys Med Rehabil.* 72,367-74.

Fisher NM and Pendergast DR (1997). Reduced muscle function in patients with osteoarthritis. *Scand J Rehabil Med*. 29:213-21.

Flanigan DC, Harris JD, Brockmeier PM, Siston RA (2010). The effects of lesion size and location on subchondral bone contact in experimental knee articular cartilage defects in a bovine model. *Arthroscopy*. 26:1655–1661.

Flanigan DC, Harris JD, Trinh TQ, Siston RA, Brophy RH (2010). Prevalence of Chondral Defects in Athletes' Knees – A Systematic Review. *Medical Science Sports Exercise.* March.

Gill T, Asnis P, and Berkson E (2006). The Treatment of Articular Cartilage Defects Using the Microfracture Technique. *Journal of Orthopaedic and Sports Physical Therapy*. 36(10):728-238.

Gomoll AH, Yoshioka H, Watanabe A, Dunn JC, Minas T (2011). Preoperative measurement of cartilage defects by MRI underestimate lesion size. *Cartilage*. October;2:389-393

Graichen H, Al-Shamari D, Hinterwimmer S, von Eisenhart-Rothe R, Vogl T, Eckstein F (2005). Accuracy of quantitative magnetic resonance imaging in the detection of ex vivo focal cartilage defects. *Ann Rheum Dis.* 64:1120-5

Hinton R, Moody R, Davis A, and Thomas S (2002). Osteoarthritis: Diagnosis and Therapeutic Conditions. *American Family Physician*.65:841-848.

Hjelle K, E. Solheim E, Strand T, Muri R, and Brittberg M (2002). Articular cartilage defects in 1,000 knee arthroscopies. *Arthroscopy*. 18(7):730-734.

Jette, AM (1980) Functional Status Index: reliability of a chronic disease evaluation instrument. *Arch Phys Med Rehabil. 61*:395-401.

Jordan JB (2001). Comparison of Four Treatments for Patients with Severe Knee Cartilage Damage. Biomedical Engineering Dept. University of Wisconsin at Madison. Retrieved from homepages.cae.wisc.edu/~jjordan/experiments/knee_treatments.html

Komistek R, Kane T, Mahfouz M, and Ochoa J (2005). Knee mechanics: a review of past and present techniques to determine in vivo loads, Journal of Biomechanics, 38(2), 215-228.

Lewis P, McCarty L, Kang R, and Cole B (2006). Basic science and treatment options for articular cartilage injuries. *Journal of Orthopaedic and Sports Physical Therapy*. 36(10):717-727.

Marcus NA (2013). Osteochondral Transplants. Virginia Cartilage Institute. Retrieved from http://www.normanmarcusmd.com/research/osteochondral-transplants

Mandelbaum B, Browne J, Fu F, Mosely B, Micheli L, Erggelet C, Minas T, and Peterson L (1998). Articular cartilage lesions of the knee. *American Journal of Sports Medicine*. 26:853-861.

McGibbon CA and Trahan CA (2003). Measurement accuracy of focal cartilage defects from MRI and correlation of MRI graded lesions with histology: a preliminary study. *Osteoarthritis Cartilage.* Jul;11(7):483-93.

Medtronic (2012). Surgical Navigation Systems. Medtronic: For Healthcare Professionals. Retrieved from http://www.medtronic.com/for-healthcare-professionals/products-therapies/spinal/surgical-navigation-imaging/surgical-navigation-systems/index.htm

Memon AR, Quinlan JF (2012). Surgical Treatment of Articular Cartilage Defects in the Knee: Are We Winning? *Advances in Orthopedics.* March.

Minas T, A. Gomall A, R. Rosenberger R, R. Royce R, and T. Bryant T (2009). Increased Failure Rate of Autologous Chondrocyte Implantation After Previous Treatment With Marrow Stimulation Techniques. *American Journal of Sports Medicine.* 37(5):902-908.

Mithoefer K, Williams R, Warren R, Potter H, Spock C, Jones E, Wickiewicz T, and Marx R (2005). The microfracture technique for the treatment of articular cartilage lesions in the knee. A prospective cohort study. *Journal of Bone and Joint Surgery, American.* 87(9), 1911-1920.

Newman AP (1998). Articular Cartilage Repair. *Am J Sports Med.* March;26(2):309-324.

Northern Digital Inc (2008). The Polaris Family of Products: Continuing a tradition of Improving Technology. *NDI P/N 8300201 (Rev.03)*.

Ong ME, Chan YH, Oh J, and Ngo A (2009). An observational, prospective study comparing tibial and humeral intraosseous access using the EZ-IO. *The American Journal of Emergency Medicine*. 27:8-15.

Papaioannou G, Demetropoulos CK, and King YH (2010). Predicting the effects of knee focal articular surface injury with a patient-specific finite element model. *Knee.* 17(1): p. 61-8.

Peña E, Calvo B, Martínez MA, Doblaré M (2007). Effect of the size and location of osteochondral defects in degenerative arthritis. A finite element simulation. *Comput Biol Med*. 37(3):376-87.

Riegger-Krugh C, McCarty E, Robinson M, and Wegzyn D (2008). Autologous chondrocyte implantation: current surgery and rehabilitation. *Clinical Sciences*. 40(2):204-214.

Scopp J and Mandelbaum B (2004). Cartilage restoration: Overview of treatment options. *Journal of Knee Surgery*. 17, 229-233.

Shah MR, Kaplan KM, Meislin RJ, and Bosco JA (2007). Articular cartilage restoration of the knee. *Bulletin of the NYU Hospital for Joint Diseases*. 65(1):51–60.

Siston R (2005). Orthopaedic Surgical Navigation: Algorithm Development and Clinical Implementation, Ph.D Dissertation, Stanford University, Stanford, CA.

Siston R, Daub A, Giori N, Goodman S, and Delp S (2005). Evaluation of Methods That Locate the Center of the Ankle for Computer-assisted Total Knee Arthroplasty. *Clinical Orthopaedics and Related Research*. 439:129-135.

Siston R, and Delp S (2006). Evaluation of a new algorithm to determine the hip joint Center. *Journal of Biomechanics*. 39:125-130.

Siston RA, Geier D, Bishop JY, Jones GL, Kaeding CC, Granger JF, Skaife T, May M, Flanigan DC (2013). The high variability in sizing knee cartilage defects. *J Bone Joint Surg Am.* Jan 2;95(1):70-5.

Siston R, Giori N, Goodman S, and Delp S (2006). Intraoperative Passive Kinematics of Osteoarthritic Knees before and after Total Knee Arthroplasty. *Journal of Orthopaedic Research*. 24:1607-1614.

Siston R, Giori N, Goodman S, and Delp S (2007). Surgical navigation for total knee arthroplasty: A perspective. *Journal of Biomechanics*. 40:728-735.

Steadman J (2001). Microfracture: Surgical Technique and Rehabilitation to Treat Chondral Defects. *Clinical Orthopaedics and Related Research*. 391SS:362-S369.

Appendix A

Optical Trackers Part Drawings

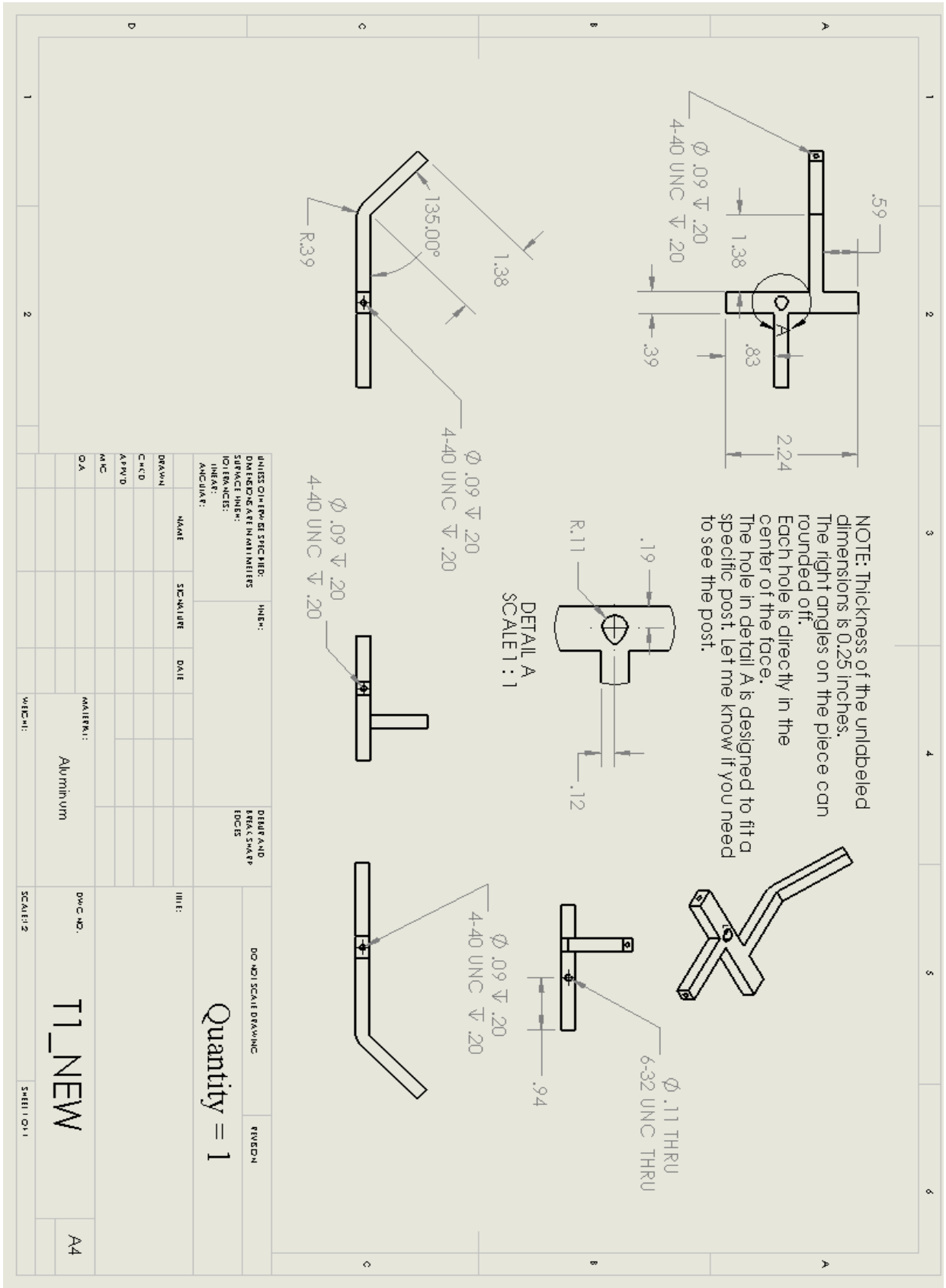

Figure A.1: Optical Tracker 1

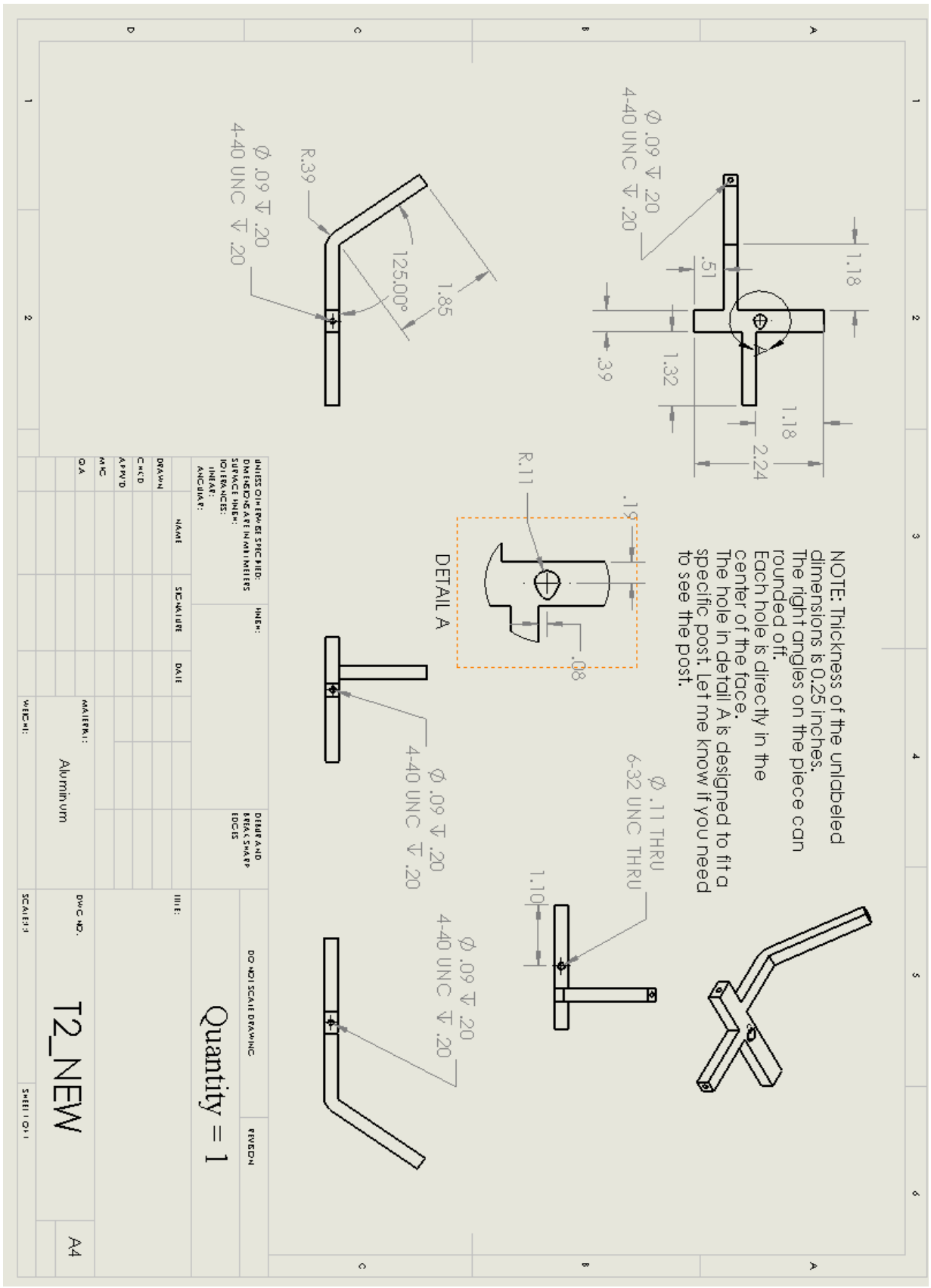

Figure A.2: Optical Tracker 2

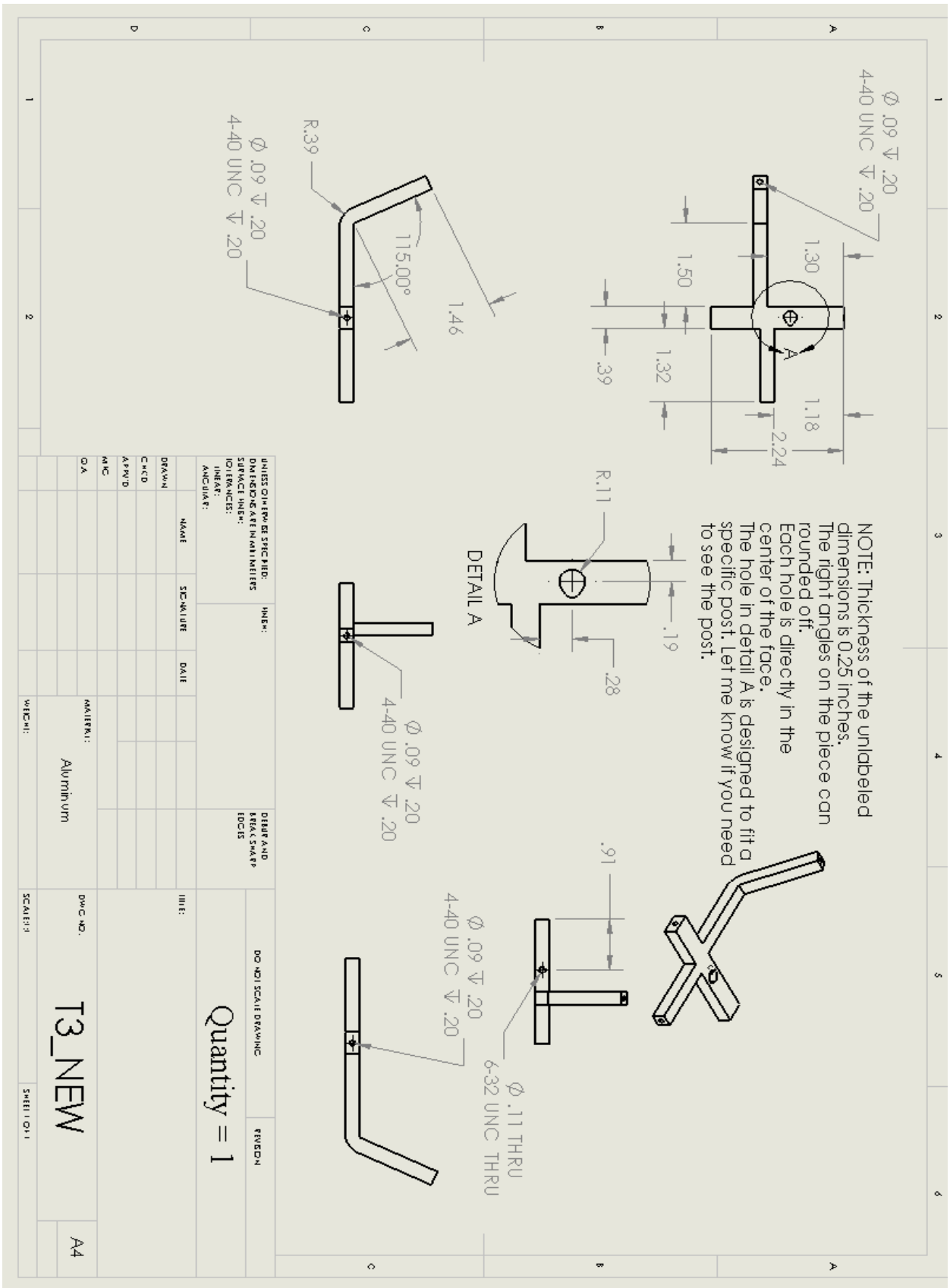

Figure A.3: Optical Tracker 3

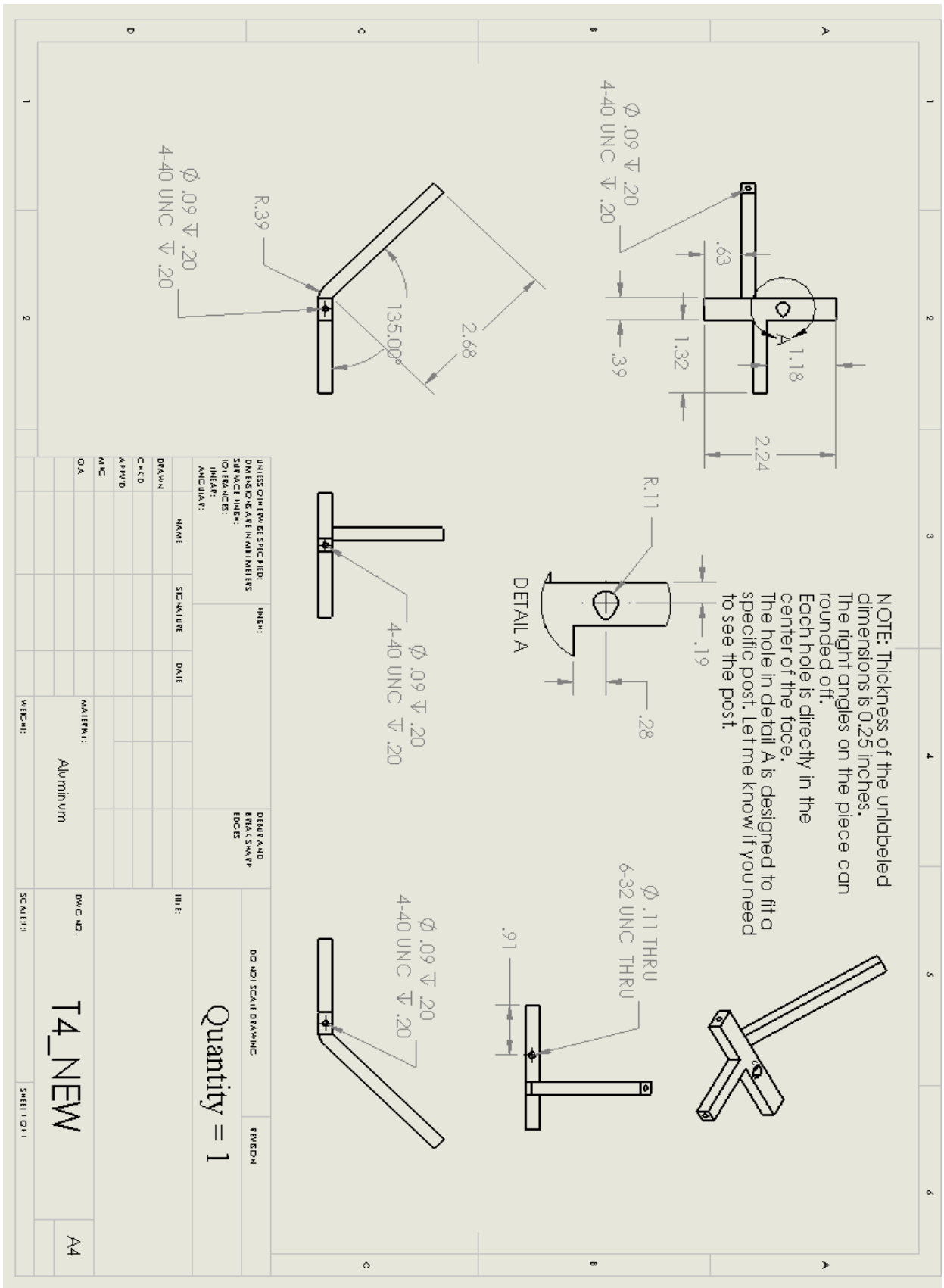

Figure A.4: Optical Tracker 4

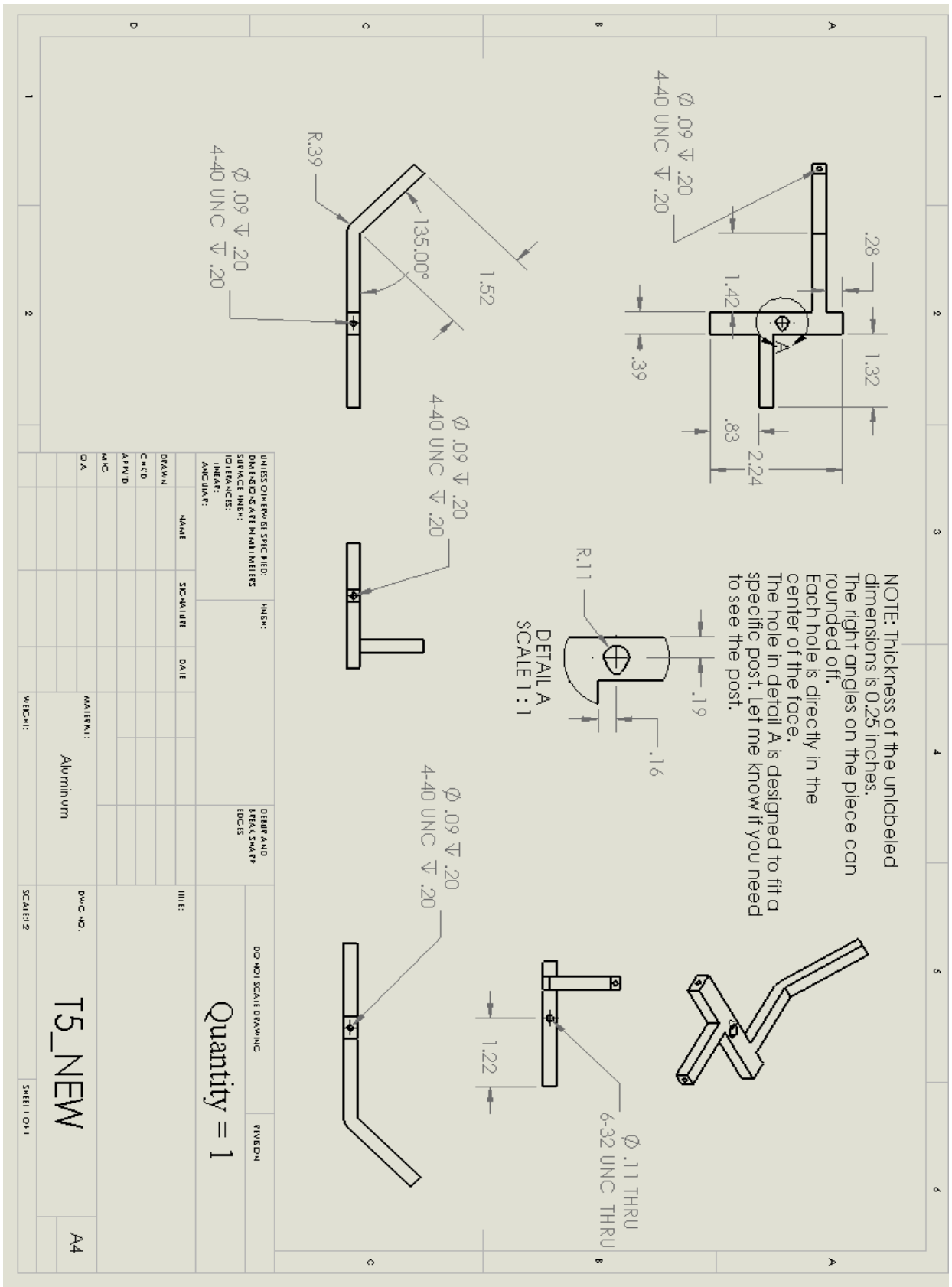

Figure A.5: Optical Tracker 5